J Ther Eng, Vol. 9, No. 1, pp. 138−160, January 2023

Journal of Thermal Engineering
Web page info: https://jten.yildiz.edu.tr
DOI: 10.18186/thermal.1243498

Journal of Thermal Engineering

Research Article

Design and analysis of an alkaline fuel cell

Mohammed AZZAM[1], Zabayyan QAQ[1], Mehmet ORHAN[1,*]

[1]*Department of Mechanical Engineering, American University of Sharjah, Sharjah, 26666, UAE*

ARTICLE INFO

Article history
Received: 17 April 2021
Accepted: 28 September 2021

Keywords:
Fuel Cell; Alkaline Fuel Cell; Thermoelectricity; Electrochemistry; Electrolyte; CFD

ABSTRACT

This study provides a step-by-step, up-to-date fuel cell fundamentals, thermodynamic and electrochemical principles, and system evaluation factors via a case study of a 10-kW alkaline fuel cell designed to operate in space applications. The system also produces 100 kg of pure water and 5.5 kW of heat. The system is modelled using MATLAB and ANSYS Fluent. Then, the model is verified with theoretical and experimental results from the literature. A parametric study of various design and operating parameters, and material selection is carried out to optimize the overall performance. A net output voltage of 0.8 V is obtained at 150 mAcm-2 current density, which yields an overall efficiency of 75%. The results indicate that increasing the electrolyte thickness or operating temperature results in a lower net voltage output. Additionally, improving the performance of a fuel cell through the bipolar plate can be achieved by understanding the contribution of different parameters towards minimizing the pressure drop across the bipolar plate. It is found that implementing an optimized selection of fluid flow rate, channel width, channel depth, number of channels and current density minimize the pressure drop throughout the bipolar plate. Relative humidity has a significant effect on the pressure drop. Results indicate that increasing the relative humidity consequentially rises the pressure drop. Finally, the CFD simulation illustrates that the end-zones in the bipolar plate accumulates fluid due to the nature of stagnation at those locations. Thus, total pressure at those locations is the highest. One of the major contributions here is studying the effect of KOH concentration on the performance of the AFC at different operating temperatures. In addition, a wide range of design and operating parameters were analysed to understand their effect on the overall performance of the fuel cell.

Cite this article as: Azzam M, Qaq Z, Orhan M. Design and analysis of an alkaline fuel cell. J Ther Eng 2023;9(1):138−160.

INTRODUCTION

Rising environmental concerns Table 1 have focused attention on developing and utilising clean and sustainable energy resources [1,2]. The aim is to develop solutions that can replace the existing fossil fuel-based power generation. Fuel cells are regarded one of the most favourable clean and efficient power generation technologies [1,2].

***Corresponding author.**
*E-mail address: morhan@aus.edu

This paper was recommended for publication in revised form by Regional Editor Liu Yang

Published by Yıldız Technical University Press, İstanbul, Turkey
Copyright 2021, Yıldız Technical University. This is an open access article under the CC BY-NC license (http://creativecommons.org/licenses/by-nc/4.0/).

Fuel cells are thermoelectric devices that transform the chemical energy of fuels into electricity without any combustion process. This one-step power generation in fuel cells replaces traditional three-step power generation. First, the fuel is burned in a combustion chamber to produce heat with greenhouse gases and pollution. This heat is then used in a heat engine to achieve mechanical shaft work. Finally, shaft work drives a generator that produces electrical power. Each of these conversion steps in the combustion chamber, heat engine, and generator sacrifices some of the energy to achieve a higher quality form, ultimately resulting in lower overall conversion efficiency. Therefore, direct and simple conversion in fuel cells offers higher efficiency with less environmental impact. Figure 1illustrates an overall fuel cell configuration with hydrogen as a fuel and oxygen as an oxidation element [3]. A cell consists of anode and cathode electrodes with an electrolyte between them. Many cells are connected together to form a stack that gives the desired current, voltage and power outputs [1,2].

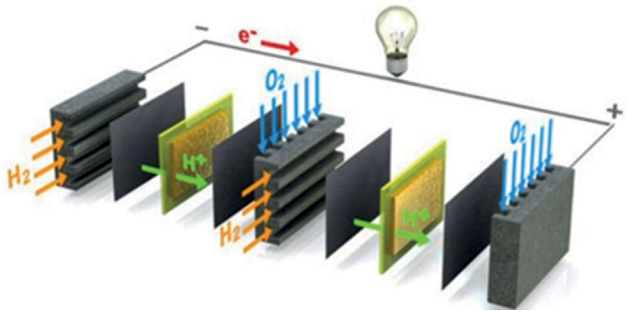


Figure 1. Overall fuel cell configuration.

Sir William Grove first introduced the fuel cell technology in 1839 by experimentally reversing a water electrolysis process. He succeeded in generating electricity in the presence of hydrogen and oxygen. The development of fuel cells continued until the beginning of the twentieth century. A major milestone was reached by Francis Thomas Bacon in 1959 when he presented the first operational fuel cell. More recently, NASA has implemented fuel cells in several space missions to utilise pure oxygen and hydrogen and generate water, electricity and useful heat output [4].

Fuel cells operate at a wide range of operating temperatures and can be implemented in different power

Table 1: Type of major pollutants & their environmental concerns

Type of Pollutants	Environmental Concerns
Particulate Matter (PM) are existing small particles containing combination of tiny liquid or solid particles. There are two types of PM Particles which are PM2.5 and PM10	1. Making lakes and streams acidic 2. Changing the nutrient balance in coastal waters and river basins 3. Damaging sensitive forests and farm crops
Sulfur Dioxide (SO2) is mainly generated from the combustion of air with fuel the contains sulfur on its chemical chain	Source for the acid rain and the environmental problems are: 1. Harmful to plant life and aquatic life 2. Causes damage to forests and vegetation 3. Corrodes statues and monuments
Carbon Monoxide (CO) is a colourless and odourless gas as a result of an incomplete combustion of fossil fuel and another carbon containing material	1. Effects the amount of greenhouse gases 2. Climate change and global warming 3. Increasing storm activity and other extreme weather events
Nitrogen Dioxide (NOx) is a reddish-brown gas which is a result of having a high combustion temperature	1. Acid rain harms sensitive ecosystems like lakes and forests 2. The nitrate particles make the air hazy and difficult to see 3. Contributes to nutrient pollution in coastal waters
Ground Level Ozone (O3) is formed by complex chemical reactions in the atmosphere.	1. Interfering with the ability of sensitive plants to produce and store food, making them more susceptible to diseases 2. Negatively impacting the appearance of urban vegetation, and vegetation in national parks and recreation areas 3. Reducing forest growth and species diversity in ecosystems
Lead (Pb) is a heavy metal usually emitted from automobiles using leaded gasoline, lead smelting and manufacturing processes	1. Lead can end up in water and soils through corrosion of leaded pipelines in a water transporting system 2. Lead accumulates in the bodies of water and soil organisms 3. Lead poisoning. Health effects on shellfish even when only very small concentrations of lead are present

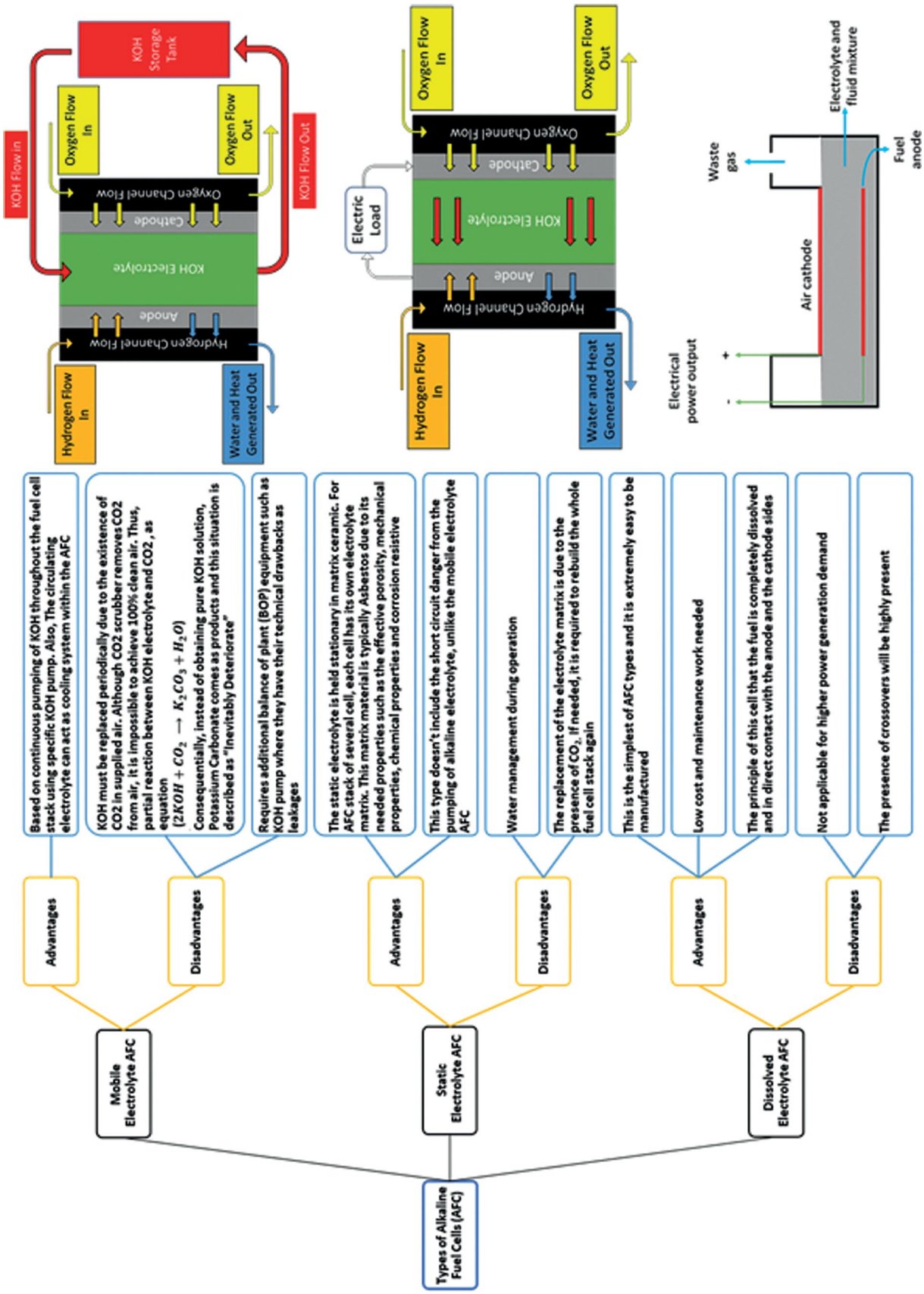


Figure 2. Comparison between the three different types of AFC.

generation applications. Due to recent enhancements, they have become alternatives to fossil fuel-based engines that produce harmful and have a significant carbon footprint on the environment [4]. Fuel cells emit low or zero levels of pollutants with higher theoretical efficiency. They can run on a wide range of gaseous and liquid fuels such as hydrogen, natural gas, methanol and gasoline [5]. Also, due to their simple and stationary process, they have a lower maintenance cost.

Five types of commercialised fuel cells are deployed with wide ranges of power output generation, temperature, pressure operating conditions and size standpoint Table 2 [4,6–13]. Figure 2 compares the three different types of alkaline fuel cell (AFC) [13].

Hydrogen production has always been a dilemma with an ongoing research and development as the current production methods are considered costly and harmful to the environment. Hydrogen is found in many substances in nature such as water, biomass, hydrogen sulphide and fossil fuels. However, it is not in its pure elemental form. It's essential to produce clean hydrogen with zero environmental impact. Below, many modern methods such as electrolysis, thermolysis, thermochemical and photovoltaic (PV) electrolysis are taken into consideration.

In electrolysis, electricity is used to generate hydrogen. Direct current is used to split water into oxygen and hydrogen. This method is the most basic process for producing pure hydrogen and oxygen from water. However, the source and production method of the electricity determines the cost and environmental impact of the electrolysis. On the other hand, in water thermolysis thermal energy is used to decompose steam at temperatures above 2500 K. Therefore, the main challenge of this method are the heat source to achieve such a high temperatures, and separating hydrogen and oxygen from the steam [14].

Thermochemical processes are also used to split water into oxygen and hydrogen. One of the major advantages of these processes is not consuming catalysis to drive the individual chemical reactions. All chemicals used in the thermochemical cycle are recycled except water, which is the material source of hydrogen. Other advantages of thermochemical water splitting cycles can be summarized as elimination of separation membranes, reasonable temperature range of 600 ~ 1200 K, and low electrical energy requirement. Due to relatively moderate temperature requirements, many sustainable thermal energy sources, such as nuclear and renewable, are available to drive the chemical reactions [14].

PV electrolysis is considered as one of the costly approaches towards producing hydrogen. Taking into consideration the available recent technologies for PV electrolysis, it is reported that the approximated cost of this method is about 25 times higher than fossil fuel alternatives. This high cost is due to the capital cost of many equipment used in the process, such as PV panels, DC bus bar, AC grid, accumulator battery set electrolyzed and hydrogen storage tank [14].

There is an ongoing effort for improvement and further commercialization of fuel cells. For instance; Verhaert, Paeppe and Mulder [15] examined the effect of increasing the air flow rate according to the increase of the electrolyte temperature in AFC. The model was developed using the control volume approach and solved the mass and energy balance of the electrochemical reactions. They concluded that raising the temperature will raise the voltage. Also, the temperature rise will increase the useful heat generation and electrical power output.

Zhang, Lin and Chen [16] performed a thermodynamic and electromechanical multifunctional model on the performance of an AFC. They considered charger-transfer, concentration and ohmic overpotentials. They found that the power output and the efficiency increased initially then decreased as the electrolyte concentration decreased. However, they found a perfect concentration value for a corresponding temperature.

Sommer, Martins, et al. [17] developed a multi-objective model to provide an accurate AFC response. The model is based on electromechanical principles, mass and species conservation. Unlike other papers, the authors analyzed the pressure drop across the gas channels. They found that an optimal value for the KOH mass fraction led to the maximum power output. Additionally, temperature gradients along the fuel and oxidation flow paths are more significant as the corresponding current density increases.

Mulder, Coenen, et al. [18] studied the effect of CO2 present in an AFC by using CO2 scrubber to decrease the CO2 concentration in the air. During the testing, a concern was raised that the stack was not utterly in an open circuit. The authors concluded that 90% of the power produced was successfully delivered to the electricity grid after eliminating CO2 and only 4% of the total power output was consumed at the primary source.

Ziems, Tannert and Krautz[19] shed light on an ambitious German government plan for transforming the country into a renewable energy provider. The target is to have 80% of the country's energy produced from renewable sources by 2050. The developed model is composed of 24 single cells connected in series using bipolar plates. The output power of the full stack was 140 kW with a maximum current density of 6 kA/m^2.

Verhaert, Verhelst, et al. [20] aimed to examine the thermal behaviour by integrating the fuel cell into a new combined heat power unit (CHP). They concluded that there is a need to reduce transmission losses by increasing the inlet air temperature and humidity. Also, that the voltage drops as the temperature drops. Similarly, at higher electrolyte temperature, the resistance, activation and diffusion losses were minimised, and the power output increased by 1% with every incremental increase of 15°C of electrolyte temperature.

Table 2: Five major commercialized types of fuel cells

Fuel cell type	Advantages	Disadvantages	Operating temperature	Typical anode/ cathode and electrolyte	Chemical equations and working fluid
Proton Exchange Membrane Fuel Cell (PEMFC)	* Relatively smaller and lighter compared to other types * Operates at low temperatures * High power density * Excellent dynamic response	* Slow reaction rates * Catalyst is made of platinum which is expensive. * Cost challenge. * Fuel supplied must be completely pure.	* 60-180°C	* Anode: Platinum supported on carbon * Cathode: Platinum supported on carbon * Electrolyte: Solid Nafion	Anode: $H_2 \rightarrow 2H^+ + 2e^-$ Cathode: $\frac{1}{2}O_2 + 2H^+ + 2e^- \rightarrow H_2O$ *Net:* $\frac{1}{2}O_2 + H_2 \rightarrow H_2O$
Direct Methanol Fuel Cell (DMFC)	* Useful for portable devices. * Operates in steady consumption of fuel and extended operating lifetime. *Simple thermal management for liquid methanol systems	* Methanol supplied causes fuel crossover and CO poisoning. * Low power density * Lack of efficient catalysts for direct oxidation of methanol	* 25-110°C	* Anode: Platinum–Ruthenium supported on carbon *Cathode: Platinum supported on carbon * Electrolyte: Solid Nafion	Anode: $CH_3OH + H_2O \rightarrow CO_2 + 6H^+ + 6e^-$ Cathode: $\frac{3}{2}O_2 + 6H^+ + 6e^- \rightarrow 3H_2O$ *Net*: $2CH_3OH + 3O_2 \rightarrow 4H_2O + 2CO_2$
Phosphoric Acid Fuel Cell (PAFC)	* Works for stationary power output with high reaction rates without the need to install expensive catalysts * Simple water management	* Difficult to start up and to deal with the electrolyte. * Low power density * Low electrical efficiencies	* 150–220°C	* Anode: Platinum supported on carbon * Cathode: Platinum supported on carbon * Electrolyte: solid ceramics	Anode: $H_2 \rightarrow 2H^+ + 2e^-$ Cathode: $\frac{1}{2}O_2 + 2H^+ + 2e^- \rightarrow H_2O$ *Net:* $\frac{1}{2}O_2 + H_2 \rightarrow H_2O$
Molten Carbonate Fuel Cell (MCFC)	* Operates with coal and fossil fuel * High electrical efficiency * Requires CO2 to operate. * Cost advantage, as it uses nonprecious metals	* Slow start up * Low power density * Corrosion of metallic parts * Catalyst dissolution in electrolyte	* 600–700°C	* Anode: Nickel Chromium * Cathode: Lithiated nickel oxide * Electrolyte: liquid alkali carbonate in Lithium aluminate	Anode (1): $H_2 + CO_3^- \rightarrow H_2O + CO_2 + 2e^-$ Cathode: $\frac{1}{2}O_2 + 2e^- + CO_2 \rightarrow CO_3^-$ *Net*: $\frac{1}{2}O_2 + H_2 \rightarrow H_2O$
Alkaline Fuel Cell (AFC)	* Achieves an overall efficiency of 70% * Cost advantage, as it can be produced by relatively standard materials * Wide range of operation temperatures	* Oxygen must be free from CO2. * Electrode flooding and drying * Extremely high sensitivity to contaminants * Low power density	* Below zero– 230	* Anode: Nickel * Cathode: Silver supported on carbon * Electrolyte: aqueous solution of Potassium Hydroxide	Anode: $2H_2 + 4OH^- \rightarrow 4H_2O + 4e^-$ Cathode: $2H_2O + O_2 + 4e^- \rightarrow 4OH^-$ *Net*: $2H_2 + O_2 \rightarrow 2H_2O + Heat$

Verhaert, Verhelst, et al. [21] aimed to develop an AFC system that can ensure extended operation time and water and thermal management. They focused on the physical flow of hydrogen, water and air. The model is divided into five areas; each has its own physical and thermodynamic behaviour. They observed that the high current requires higher electrolyte temperatures to maintain the concentration.

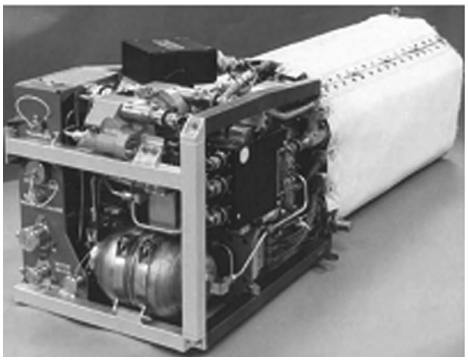
Jiao, Huo, et al. [22] developed an AFC analytical model. The model solved the mass balance equations for the derivations of cell voltage, current and power output. They considered the effect of operating pressure, cathode humidification and membrane thicknesses. They found that humidifying the cathode will improve the performance and increase the voltage until activation and ohmic losses decrease. The stoichiometry ratio did not affect the performance at low current densities. However, at higher current densities, decreasing the stoichiometric ratio enhances the cell performance. Decreasing operating pressure will improve the voltage and performance at higher current densities. The thickness of both membrane and catalyst layers affects the voltage losses; thicker layers will increase the losses and decrease the cell voltage. Finally, cathode humidification has a significant effect on performance due to electrochemical reaction.

Ariyanfar, Ghadamian and Roshandel[23] examined the performance of a mobile AFC with operating conditions influenced only by the presence of the electrolyte. They obtained the optimum current after varying the voltage losses, and the heat transfer between the plates and the environment was calculated. The relationship between the voltage and the current density was affected by the irreversibility, and the cell current increase causes a drop in voltage because of the losses. The electrolyte flow rate and pressure drop are two parameters that can influence the overall performance of the fuel cell.

Lin, Kirk and Thorpe [24] studied the effect of the materials selected for the anode and cathode and visualised the effect of the operating conditions on the overall performance. The maximum value of the electrolyte concentration must be maintained at 8 M to achieve ionic conductivity. When achieving a higher current and voltage output due to the enhancement of the reaction kinetics with the increase of temperature, the conductivity rises, but the ohmic polarisation decreases.

Despite the low amount of research in this type of fuel cells, this research selected this topic because the AFC shows some interesting prospects such as cheaper construction. Also, It can be produced by relatively standard materials and does not require expensive metals [6]. However, this specific fuel cell technology approach has not made expected progress or achieved dominance in the technology of clean energy power generation. Most AFC-expert researchers agree that the main cause of this

Table 3: Different models of NASA's AFC

Spacecraft name	Space Shuttle Orbital	Apollo Spacecraft
Picture of the Fuel Cell		
Year of Application	1980s	1960s
Overall Power Output	12 kW	1.5 kW
Number of Cells	32 cells	31 Cells
Output Voltage	0.875 V	0.860 V
Working Temperature	93°C	230°C
Working Pressure	0.41 Mpa	0.34 MPa
Electrolyte Configuration	Static	Static
External Dimensions	36 × 38 × 114 cm	111.76 × 55.88 × 55.88 cm
Net Weight	120 kg	113 kg

slow progress is adopting the liquid solution of alkaline electrolyte [25]. This analysis of KOH was implemented in forward sections. NASA has implemented AFCs during several space exploration missions because it can achieve an overall efficiency of 70%. The space mission that implemented an AFC was the Apollo program. AFC batteries are still used in the space shuttle to supply electricity at a power of between 2 kW and 12 kW (the maximum power is 16 kW) and an overall voltage between 28 V and 32 V [12]. Table 3compares two models of AFCs in the Apollo program [25].

To help aforementioned ongoing efforts, the objective of this study is to provide a comprehensive review of fuel cell technology focusing on alkaline fuel cells (AFCs). Also, to present a step-by-step approach to model an alkaline fuel cell using the fundamentals, thermodynamic, electrochemical principles, and system evaluation factors via an application of a 10-kW alkaline fuel cell designed to operate for one day in a space application. To model the system using MATLAB and ANSYS Fluent Computational Fluid Dynamics (CFD). To start with, MATLAB is utilized to numerically perform a parametric study of various designs and operating conditions such as inlet and outlet conditions; in order to visualize the performance across wide ranges of parameters. Variation the overall performance with operating temperature, thickness of cell components, humidification and KOH concentration is analysed. Then, ANSYS Fluent is utilized to visualize the bipolar plate performance from material selection and boundary conditions perspective. The theoretical results obtained in this work are verified with theoretical and experimental results from the literature. The main novelty and contribution of the study is evaluating the effect of KOH concentration on the performance of an AFC at various operating temperatures, and analysing many design and operating parameters simultaneously to evaluate their interrelation, which lacks in the literature.

MODEL DESCRIPTION

The fuel cell that will be modelled in this paper is an AFC. AFC has an aqueous solution of potassium hydroxide as an electrolyte (KOH). Although it is necessary that both the hydrogen used at the anode and the oxygen used at the cathode side be free from CO2 as it is a major requirement for the operation of an AFC, the chemical equations within the fuel cells are different. However, it is still considered as an oxidation-reduction reaction between hydrogen and oxygen [6]. Figure 3 displays the chemical equations of an AFC on each side of the fuel cell.

The following assumptions are applied:

1. The anode is supplied with pure hydrogen in gaseous form
2. The cathode is supplied with atmospheric air (79% nitrogen and 21% oxygen) at Pr=0.7
3. The cathode is fully humidified before direct injection to the cell
4. The flow is laminar, steady state, with a low Reynolds number
5. Ideal gas assumption
6. The operating temperature and pressure are held unchanged across the flow streams
7. Water generated is in liquid form (higher heating value)
8. The heat transfer losses from the gas flow channels to the environment are negligible
9. Gravity was considered in CFD analysis to visualize buoyancy effect

Selecting the proper material with suitable dimensions have a significant effect on the outcome. The anode and cathode are made of carbon supported by a nickel catalyst, and silver catalyst, respectively. Nickel is used due to its ability to reduce the rate of activation energy at the anode. When silver is introduced to the cathode as a supported catalyst, it boosts the reaction at the cathode side. The gas diffusion layer (GDL) can be either carbon paper or carbon cloth. Both are carbon fibre-based porous material. Carbon paper is non-woven, while carbon cloth is a woven fabric. There are no major differences between these two types of carbon fibre materials; in this model, carbon paper is selected. The arrangement of these carbon fibres can be used to ensure electrical conductivity for current collection pathway, provide a connection for the bipolar plate with channel-land structure and electrode and protection for catalyst layer from carrion or erosion by flow.

Bipolar plates can be made of graphite, stainless steel, or ceramics. Stainless steel is selected [3]. The coating material varies between Ti-Co and $TiCo_3$. $TiCo_3$ will be selected for the strong bending with stainless steel [26]. The external manifold will be aluminium due to its strength and light weight. The internal layers starting from the anode endplate to the cathode endplate are shown in Figure 3.

Balance of plant (BoP) governs all the auxiliary components within the whole fuel cell system except the stack itself (the anode, cathode, electrolyte, etc.). These components can be pumps, heat exchangers, compressors, blowers, or humidifiers [27]. The cell uses four main streams: air, hydrogen, KOH and water production. Each stream will require certain components for operation. The BoP configuration is shown in Figure 4 The hydrogen line contains the hydrogen tank which stores pressurised hydrogen gas and a pressure reducing valve to release pressure to the desired operating pressure. The air line contains the air tank to store air. This tank is connected to a CO_2 scrubber to purify the air, and then the purified air is supplied to the system using an air fan. The KOH solution is stored in a KOH tank, and it was circulated within the system using a specific KOH pump. Finally, the water produced is used to cool the fuel cell stack and then pumped back to the water tank.

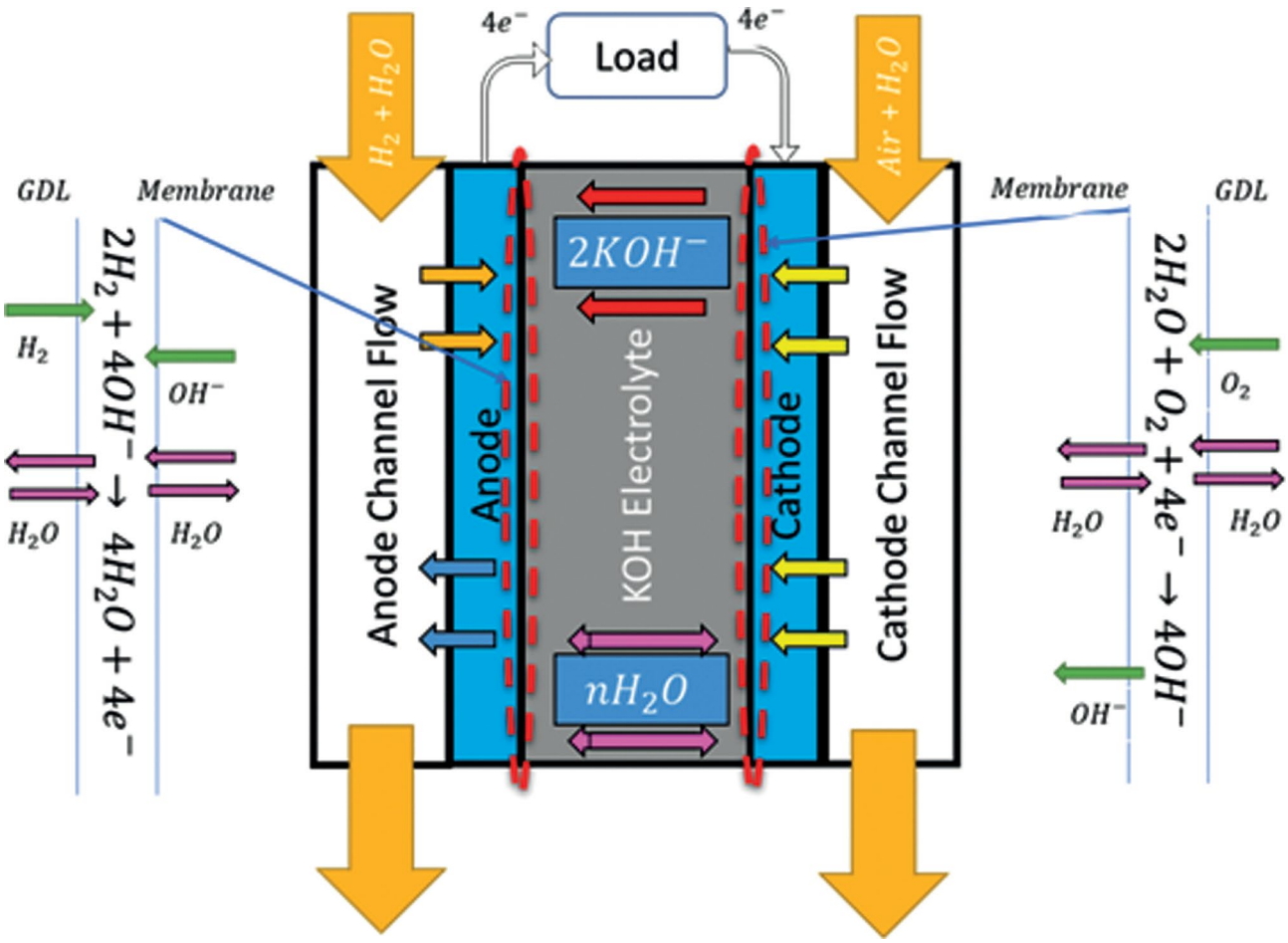


Figure 3. AFC chemical equation on each side.

The major operating parameters such as the temperature and pressure of the fuel and the air (or oxygen) are summarized in Table 4. The electrode consists of two layers, a diffusive layer and a reactive layer. The diffusive layer provides gas uniformly, and the reactive layer removes the by-products of the reaction. The diffusive layer is made of hydrophobic material.

Bipolar plates (BP) are a key component with a multifunctional character. BP uniformly distributes fuel gas and air, conduct electrical current from cell to cell, remove heat from the active area, and prevent leakage of gases and coolant [28]. BP separates the adjacent cells if more than one cell is connected. In addition, they act as a current collector of the chemical reaction. Finally, they feed the air or pure oxygen to the anode and fuel to the cathode. Figure 5 shows the bipolar plate. The holes are the inlet and outlet face for the flowing fluid. The zoomed view to the right shows how the channel width, depth and height are represented.

Manifolds enable a low-pressure drop and good flow distribution within the fuel cell layer, but they have a disadvantage, which is 'crossflow'. Due to the crossover, unequal and nonuniform temperature distribution and gas leakage of the flows can occur [29]. There are two types of manifolds: external and internal. External manifolds do not provide cooling within the fuel cell stacks. Internal manifolds introduce an additional flow of fluids within the fuel cell

Table 4: Main parameters and assumptions.

Name of Parameter	Numerical Value
Operating hours (Life-time)	24 hours (1 day)
Fuel cell operating temperature	T = 85°C = 358.15 k
Inlet pressure of hydrogen	P_{H_2} = 2 *atm*
Inlet pressure of oxygen	P_{O_2} = 3 *atm*
Outlet pressure of water produced	P_{H_2O} = 2 *atm*
Power output (total)	P = 10,000 W
Number of cells	n = 30 cells
Humidity at the inlet air	φ = 90%
Stoichiometry ratio of hydrogen	λ_{H_2} = 1
Stoichiometry ratio of oxygen	λ_{O_2} = 1.5

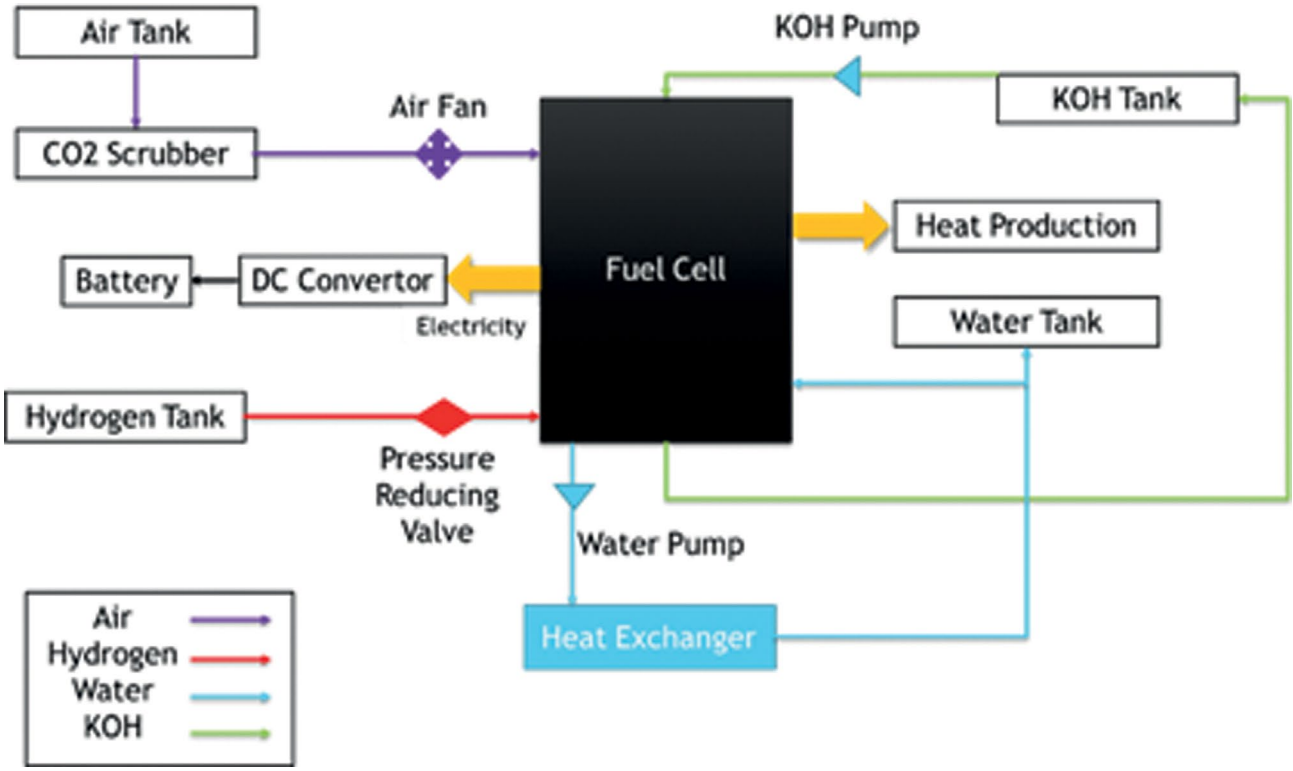


Figure 4. Balance of plant (BoP) configuration.

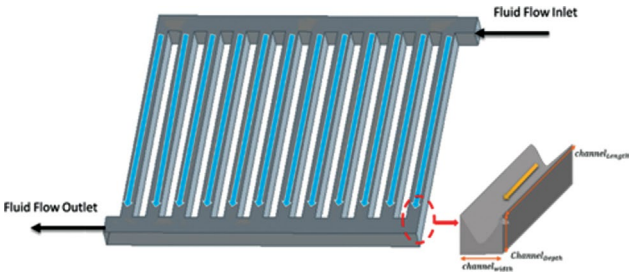


Figure 5. Bipolar plates cross-sectional view.

stacks [3]. It is critical to ensure the perfect material selection for the external manifolds (endplates) to withstand the compressive forces away from the internal body of the fuel cell. The range for the material selection available can extend from a low to high operating temperature and for a small and large fuel cell. Some of the commonly used materials are graphite, stainless steel, aluminium and nickel. Aluminium is selected due to its light weight and strength. Figure 6 shows the flow chart of the design procedure and validation of the AFC results.

ANALYSIS

Gibbs free energy 'ΔG' is the energy available to perform external work, neglecting any work done by changing temperature or volume. Specific heat obtained in equations (1) to (3) [30]

$$(c_p)_{Steam} = 143.05 - 58.040T^{0.25} + 8.2751T^{0.5} - 0.036989T \quad (1)$$

$$(c_p)_{Hydrogen} = 56.505 - 22{,}222.6T^{-0.75} + 116{,}500T^{-1} - 560{,}700T^{-1.5} \quad (2)$$

$$(c_p)_{Oxygen} = 37.432 + 2.010210^{-5}T^{1.5} - 178{,}570T^{-1.5} + 2{,}368{,}800T^{-2} \quad (3)$$

The total enthalpy and entropy are, according to equations (4) and (5),

$$(h_T) = h_{ref} + \int_{298.15}^{T}\left(\frac{1}{T}\right)c_p dt \quad (4)$$

$$(S_T) = s_{ref} + \int_{298.15}^{T}\left(\frac{1}{T}\right)c_p dt \quad (5)$$

$\Delta H_{\substack{Enthalpy\ of \\ Formation}}$ and $\Delta H_{\substack{Total \\ Entropy}}$ for the net chemical reaction for AFC from equations (6) and (7).

$$\Delta H_{Formation} = (\Delta H_{Products}) - (\Delta H_{Reactors}) \quad (6)$$

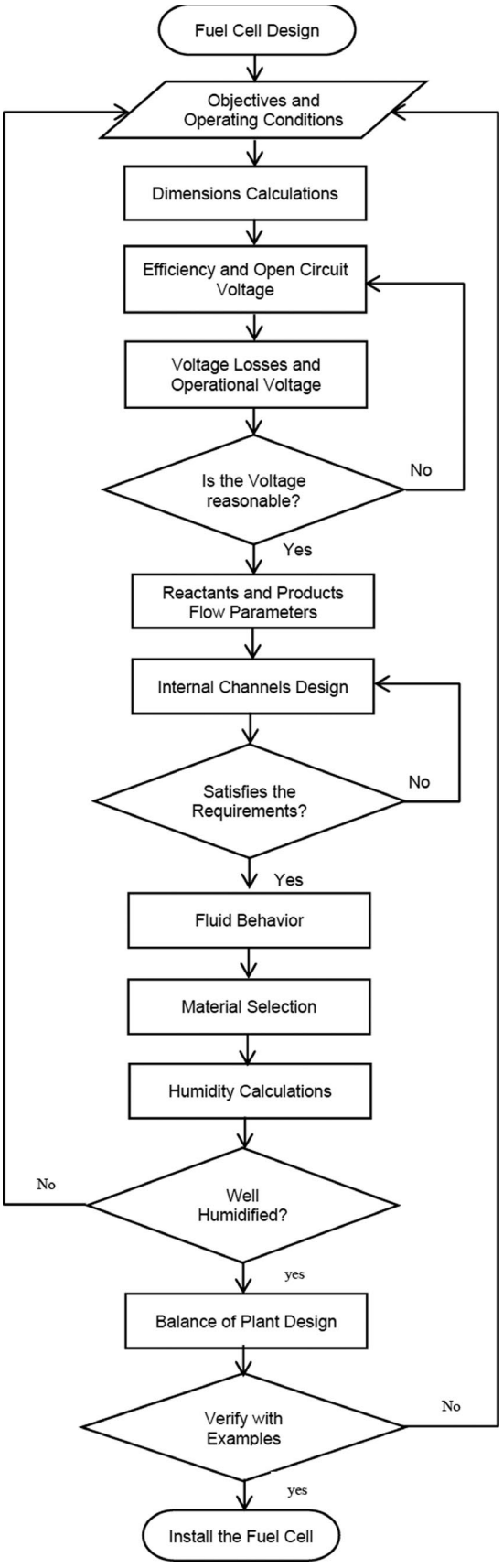


Figure 6. Flow chart of the AFC design procedure.

$$\Delta S_{Entropy} = (\Delta S_{Products}) - (\Delta S_{Reactors}) \quad (7)$$

The Gibbs free energy per moleis shows in equation (8).

$$\Delta G = \left(\Delta H_{\substack{Enthalpy\ of \\ Formation}}\right) - T\left(\Delta S_{\substack{Total \\ Entropy}}\right) \quad (8)$$

The maximum voltage achieved without the presence of voltage losses internally (also known as the no loss voltage), is called the electromotive force (EMF) according to equation (9):

$$EMF = \left(\frac{-\Delta g_f}{zF}\right) \quad (9)$$

The effect of the pressure and gas concentration at the anode and cathode is found using equations (10) and (11) to obtain the enhanced EMF (open-circuit voltage (OCV)) and enhanced Gibbs free energy:

$$E_{OCV} = E^o + \left(\frac{RT}{2F}\right) ln\left(\frac{P_{H_2}(P_{O_2})^{1/2}}{P_{H_2O}}\right) \quad (10)$$

$$G_{OCV} = G^o + (RT) ln\left(\frac{P_{H_2}(P_{O_2})^{1/2}}{P_{H_2O}}\right) \quad (11)$$

The theoretical conversion efficiency (thermodynamic efficiency) is calculated using the reference value of higher heating value (HHV) of the fuel. The efficiency of the fuel cell is obtained from equation (12):

$$Efficiency = \mu_f \left(\frac{\Delta G_f}{\Delta H_f}\right) \times 100\% \quad (12)$$

μ_f is the fuel utilisation factor. It is reasonable to assume the fuel utilisation factor to be between 0.9 and 0.95.

The activation losses at the anode and cathode due to the slowness of the reactions taking place at the electrode surface can be expressed as equation (13). is the internal current density [15].

$$\left(\Delta V_{act}\right) = \left(\frac{RT}{2\alpha F}\right)\left[ln\left(\frac{i+i_x}{i_{o_a}}\right) + ln\left(\frac{i+i_x}{i_{o_c}}\right)\right] \quad (13)$$

Ohmic losses are due to the resistance of the flow of ions in the electrolyte and electrons. They can be expressed according to equation (14):

$$(\Delta V_{ohm}) = iA_{cell}\left(\frac{\frac{l_a}{A_{cell}\sigma_a} + \frac{l_e}{A_{cell}\sigma_e} + \frac{l_c}{A_{cell}\sigma_c} + \frac{R_a}{\left(\frac{A_{cont}}{LW\ Ratio}\right)} + \frac{R_C}{\left(\frac{A_{cont}}{LW\ Ratio}\right)}}{}\right) \quad (14)$$

One approach takes half of the thickness for anode and cathode, as the reaction will not take place along the whole layer. The contact resistance value for the anode and the cathode are $R_a = 10 \times 10^{-3}\ \Omega cm^2$ [31] and $R_c = 6 \times 10^{-6}\ \Omega cm^2$ [32].

Mass transport loss is due to a decrease in reactant concentration at the surface of the electrode as fuel is consumed. Mass transport is expressed using the practical approach in equation (15):

$$(\Delta V_{trans}) = me^{ni} \tag{15}$$

The net voltage, considering the three different types of losses, is expressed in Equation (16):

$$\mathrm{V} = E_{OCV} - (\Delta V_{act}) - (\Delta V_{ohm}) - (\Delta V_{trans}) \tag{16}$$

The current value is calculated according to the net voltage [31] using equation (17).

$$A_{cell} = \frac{Current}{Current\ Density} \tag{17}$$

Fluid usage is defined as the minimum amount of fluid supply needed to run the fuel cell. Air, hydrogen and oxygen use are calculated according to equations (18) to (20):

$$O_{2'usage} = \frac{In}{4F} \tag{18}$$

$$H_{2'usage} = \frac{In}{2F} \tag{19}$$

$$Air\ Supply\ (Usage) = 3.57 \times 10^{-7}(\lambda_{O_2})\left(\frac{P_e}{V_{cel}}\right) \tag{20}$$

The molar rates and the mass flows rate are obtained according to equations (21) and (22):

$$(\dot{n})_{H_2,O_2} = n\lambda\left(\frac{iA}{nF}\right) \tag{21}$$

$$(\dot{n})H_2O = (\dot{n})_{H_2} \tag{22}$$

Stoichiometric ratios are always used in operational fuel cells. Equation (23) is used to calculate the unreacted oxygen [34]. Because the ratio for hydrogen equals one, all the hydrogen let into the cell will react.

$$\lambda_{O_2} = \frac{(m_{O_2})_{actual}}{(m_{O_2})_{required}} \tag{23}$$

The water and heat production are obtained according to equations (25) and (26):

$$Water\ Production = 9.34 \times 10^{-8} \times \left(\frac{P_e}{V_{cel}}\right) \tag{24}$$

$$Heat\ Production = P_e\left(\frac{1.25}{V_{cel}} - 1\right) \tag{25}$$

The bipolar plate is where the channels are placed that host the flow of working fluids [33].equations (26) to (32) are used [4] to calculate the stack's inlet volumetric flow rates, velocities, hydraulic diameter, Reynolds number, friction drop factor and pressure drop:

$$Q_{Hydrogen} = \left(\frac{I\lambda RT_{in}N_{cell}}{2Fr(P_{in} - \varphi P_{sat@T_{in}})}\right)_{Hydrogen} \tag{26}$$

$$Q_{air} = \left(\frac{I\lambda RT_{in}N_{cell}}{2Fr(P_{in} - \varphi P_{sat@T_{in}})}\right)_{air} \tag{27}$$

$$(Q_{stack,in})_{O_2} = 0.21(Q_{stack,in})_{air} \tag{28}$$

$$(V_{avg}) = \frac{Q_{stack,in}}{Cells N_{channels} A_{CS_{channel}}} \tag{29}$$

$$D_h = \frac{2w_c d_c}{w_c + d_c} \tag{30}$$

$$f = \frac{55 + 41.5\left(e^{\left(\frac{-3.4}{\frac{w_c}{d_c}}\right)}\right)}{Re} \tag{31}$$

$$\Delta P = \left(f\frac{L}{D_H}\right)\left(\frac{\rho(v_{avg})^2}{2}\right) + \Sigma K_L\left(\frac{\rho(v_{avg})^2}{2}\right) \tag{32}$$

Water pressure at 85°C is obtained from equations (33) and (34). The fuel cell can be either too dry if the relative humidity is less than 80%, or too wet if the relative humidity is over 100%. Because, it is a well-humidified fuel cell according to Figure 7 [30]:

$$P_w = \left(\frac{0.42}{\lambda_{O_2} + 0.21}\right)P_{w,e} \tag{33}$$

$$RH = \frac{P_w}{P_{sat}} \tag{34}$$

The electrolyte concentration of the fuel cell is expressed in terms of molarity (mol/L). Understanding the effect of the concentration by using ohmic losses [15]according to equations (35) to (37) is used to achieve the desired output voltage by varying the concentration of the electrolytes.

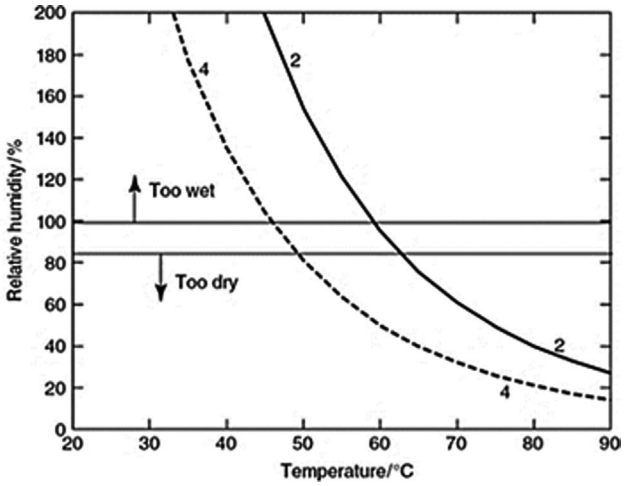


Figure 7. Plot of relative humidity vs. exit temperature.

$$U_{ohm} = i\frac{t}{k} \tag{35}$$

$$M_{opt} = 159.79(50.0056 + 6\times10^{-7}T^2 - 6 \times 10^{-7}\sqrt{\frac{(T^2 - 583.156T + 89464.7)}{(T^2 + 775.559T + 418493)(T - 192.403)}{T}}) \tag{36}$$

$$k = \frac{-2.041M - 0.0028M^2 + \frac{207.2M}{T} + 0.001043M^3 - 0.0000003M^2T^2}{100} \tag{37}$$

Estimated total system volume was obtained by calculating the sum of all volumes of the components of the fuel cell according to Equations (38) and (39):

$$Volumetric\ Power\ Density = \frac{Power(kW)}{System\ Volume(m^3)} \tag{38}$$

$$Gravimetric\ Power\ Density = \frac{Power(kW)}{System\ Mass(m^3)} \tag{39}$$

An ANSYS FLUENT CFD simulation was carried out for the bipolar plate accounting for the properties of air during the lifetime of the fuel cell. This type of bipolar plate used is called the parallel flow field. Thus, the first step is to build well-distributed mesh cells with the optimum element quality. The mesh selection has to undergo a mesh independence validation, where every run will have different mesh elements sizes. This step will be repeated till no noticeable difference in the results is obtained. Thus, it can be concluded that the solution in mesh size independent.

Table 5. Pressure drop obtained for each mesh element size and its percentage error

Element Size (mm)	Pressure Drop (Pa)	Percentage Error (%)
3	0.173038528	[–]
2	0.183479615	6.03%
1.5	0.185396184	1.04%
1	0.187798	1.30%
0.75	0.188449286	0.35%
0.5	0.18855803	0.06%

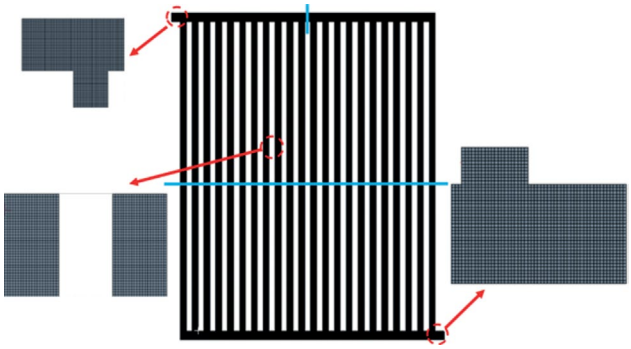


Figure 8. Mesh mapping of bipolar plate.

The mesh independence validation will take place at two different locations on the bipolar plate geometry; the middle point of the inlet channel and the middle of the vertical parallel channels towards the outlet. Figure 8shows the mapped mesh used. The red circles indicate three different locations to visualise the good distribution of the mesh cells. The light blue lines show the location where the mesh independence validation took place. Another approach to ensure the accuracy of the mesh is obtaining the pressure drop across the bipolar plate. Figure 9 and Figure 10shows the results for the different elements sizes runs used in the mesh independence validation at the middle point of the inlet channel and vertical walls, respectively. For Figure 9, similar results were obtained showing the velocity profile at that point [34]. Also, similar results for Figure 10 were found in [35] which provided the velocity magnitude at the vertical parallel channels. Percentage difference was calculated to compare the different element sizes. Table 5 shows the calculations for the pressure drop for each mesh element size. The number of mesh elements selected 511,000 with an average element quality of 0.99946. The solution method scheme used in this simulation is the coupled scheme. Second order upwind is used as the spatial discretization for the energy, momentum and pressure. While least square cell based is used as the spatial discretisation for the gradient. The relaxation factors used in this simulation are

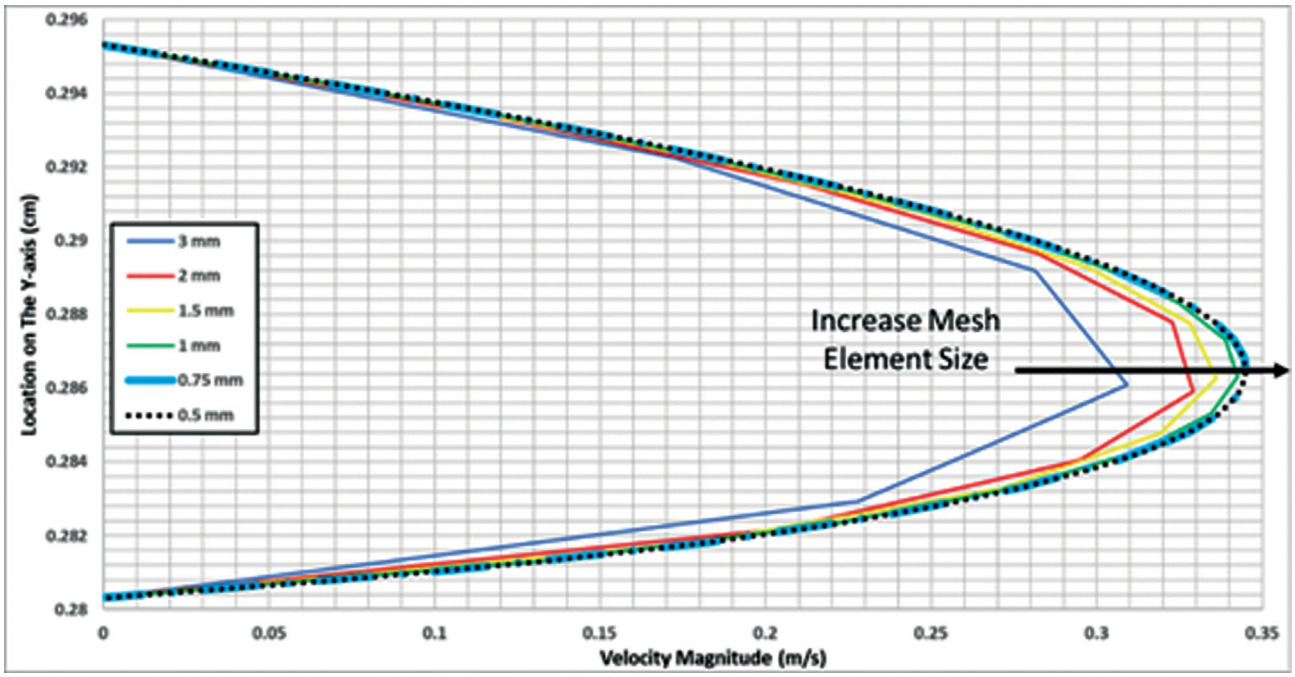


Figure 9. Mesh independence validation for the first location on the mesh map.

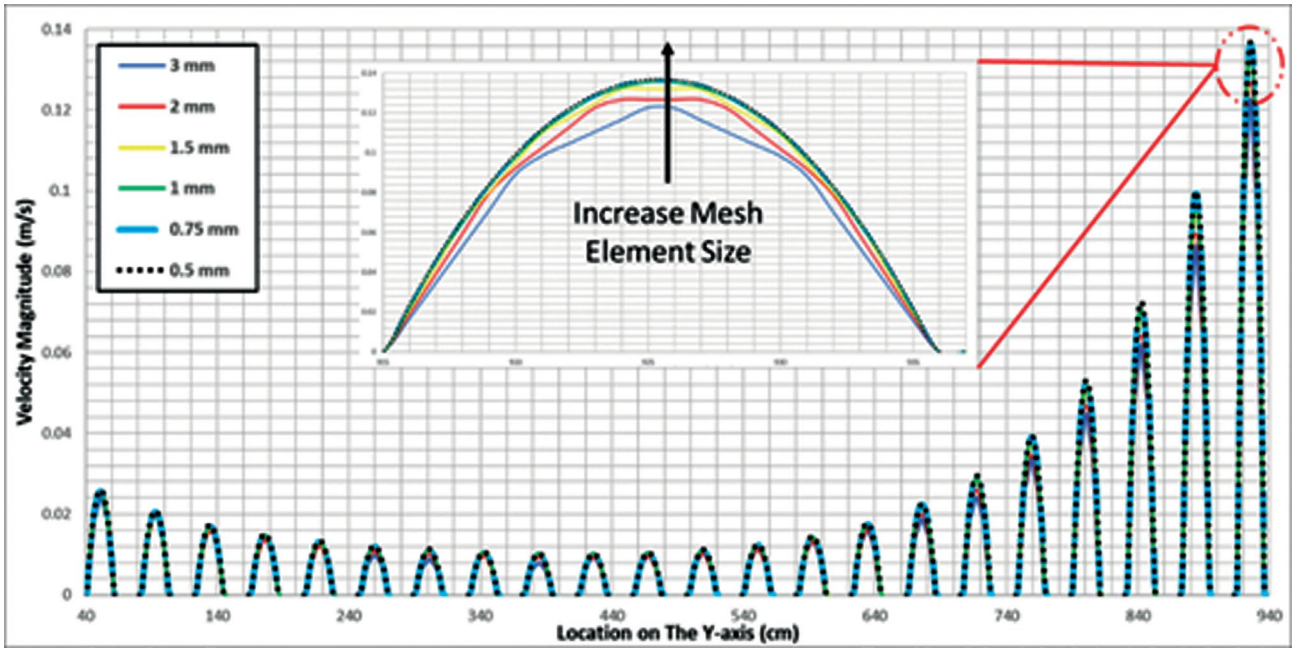


Figure 10. Mesh independence validation for the second location on the mesh map.

0.5 for the pressure and momentum, 1 for the density and body force, and 0.75 for the energy. The residual criteria for continuity, momentum and energy are all set to 1×10^{-9}. Convergence was achieved for all element sizes after almost 100 iterations.

The CFD governing equations that will be used for the simulation are the conservation of momentum equation, Compressible fluid continuity equation and energy equation are shown in equations (40) to (44), respectively.

$$u\frac{\partial u}{\partial x}+v\frac{\partial u}{\partial y}+w\frac{\partial u}{\partial z}=-\frac{1}{\rho}\frac{\partial P}{\partial x}+\frac{\mu}{\rho}\left(\frac{\partial^2 u}{\partial x^2}+\frac{\partial^2 u}{\partial y^2}+\frac{\partial^2 u}{\partial z^2}\right)+g_x \quad (40)$$

$$u\frac{\partial v}{\partial x}+v\frac{\partial v}{\partial y}+w\frac{\partial u}{\partial z}=-\frac{1}{\rho}\frac{\partial P}{\partial y}+\frac{\mu}{\rho}\left(\frac{\partial^2 v}{\partial x^2}+\frac{\partial^2 v}{\partial y^2}+\frac{\partial^2 v}{\partial z^2}\right)+g_y \quad (41)$$

$$u\frac{\partial w}{\partial x}+v\frac{\partial w}{\partial y}+w\frac{\partial w}{\partial z}=-+\frac{1}{\rho}\frac{\partial P}{\partial z}+\frac{\mu}{\rho}\left(\frac{\partial^2 w}{\partial x^2}+\frac{\partial^2 w}{\partial y^2}+\frac{\partial^2 w}{\partial z^2}\right)+g_z \quad (42)$$

$$\frac{\partial(\rho u)}{\partial x}+\frac{\partial(\rho v)}{\partial y}+\frac{\partial(\rho w)}{\partial z}=0 \quad (43)$$

$$k_m\left(\frac{\partial^2 T}{\partial x^2}+\frac{\partial^2 T}{\partial y^2}+\frac{\partial^2 T}{\partial z^2}\right)=0 \quad (43)$$

The mesh created for each mesh element size will be evaluated according to mesh quality, which takes into account the length of each element in the map. Network quality can be calculated from equation (45)

$$Quality = C\left[\frac{volume}{\sqrt{\{\sum(Edge\ legth)^2\}^3}}\right] \quad (45)$$

RESULTS AND DISCUSSION

As it was stated before, MATLAB and ANSYS Fluent were used to study the effect of the operating parameters and draw a conclusion about the influence on the overall performance of the fuel cell. The operating parameters include variation in operating temperature, electrolyte thickness, inlet humidity and KOH concentration. These results were verified by previously published papers and AFC experimental related works.

Overall Fuel Cell Performance Analysis

Figure11 shows the effect of operating temperature on the theoretical cell efficiency and Gibbs free energy. From the Figure, the cell efficiency is inversely proportional to the operating temperature. Thus, lower operating temperatures leads to a better dynamic response while start-up [4]. The results in Figure 11 are theoretical. Yet, in real-life applications, the increase in the operating temperatures will result in increasing the voltage. Because at higher temperatures the gas diffusivity and membrane conductivity increases, activation losses reduce [36]. Also, the relation between Gibbs free energy and the operating temperature is directly proportional

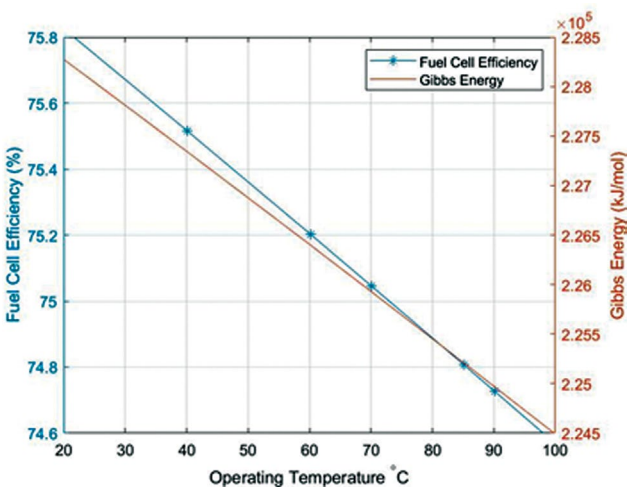


Figure 11. Plot of theoretical cell efficiency & Gibbs free energy vs. the operating temperature.

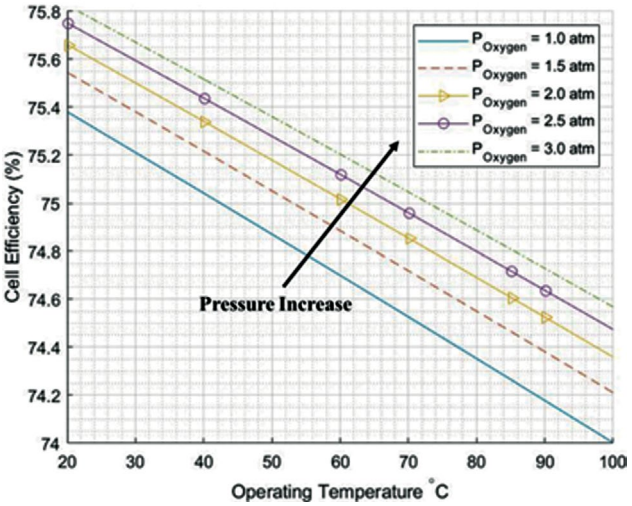


Figure 12. Plot of cell efficiency and the variation of oxygen pressure at different temperatures.

to the negative side. That is increasing the numerical value of temperature will decrease the Gibbs free energy.

The increase in fluid inlet pressure will enhance the output cell voltage, which will also enhance the efficiency of the AFC as shown in Figures 12 and 13. Similar findings were theoretically obtained in [37,38].

Figure 14 shows the theoretical relationship between the power output of the system with variation of electrolyte thickness. The generated power increases as the current density increases to a certain current density (around 1 Acm^{-2}). Then, the power output starts to decrease after the peak point. Also, when electrolyte thickness increases, the power output decreases. This because increasing the electrolyte thickness, will result in increasing the ohmic losses,

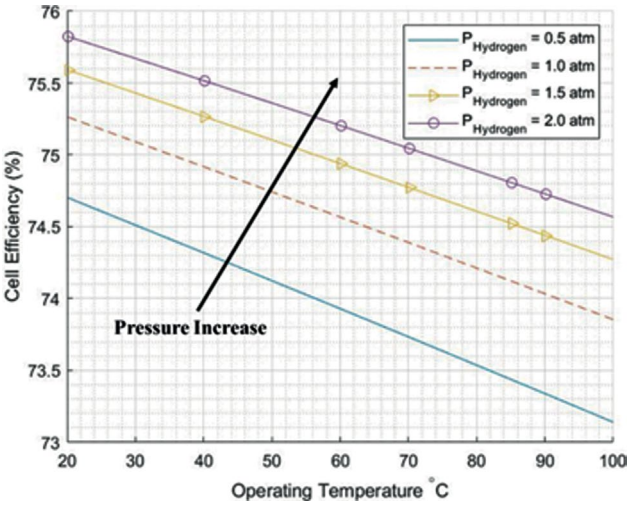


Figure 13. Plot of cell efficiency vs. the variation of hydrogen pressure at different temperatures.

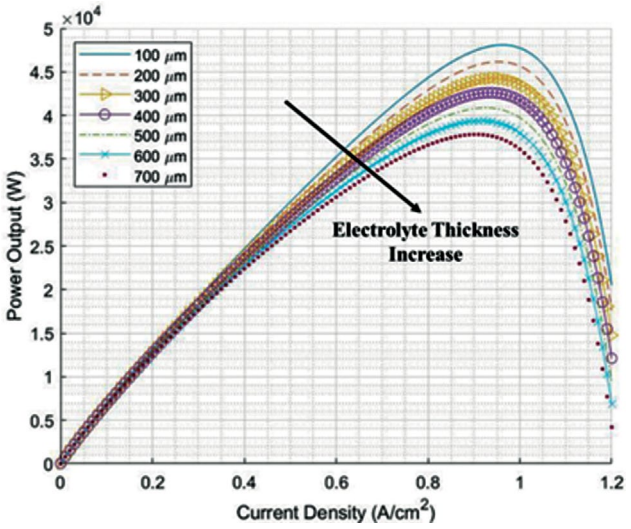


Figure 14. Plot of power output vs. current density.

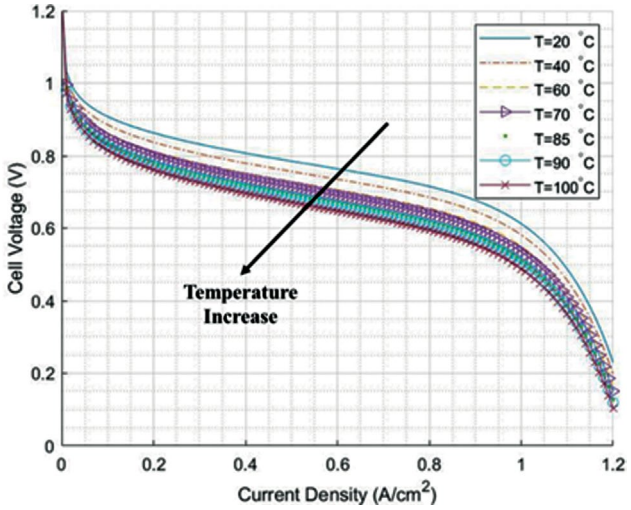


Figure 15. Plot of polarization curve with variation of Operating Temperature.

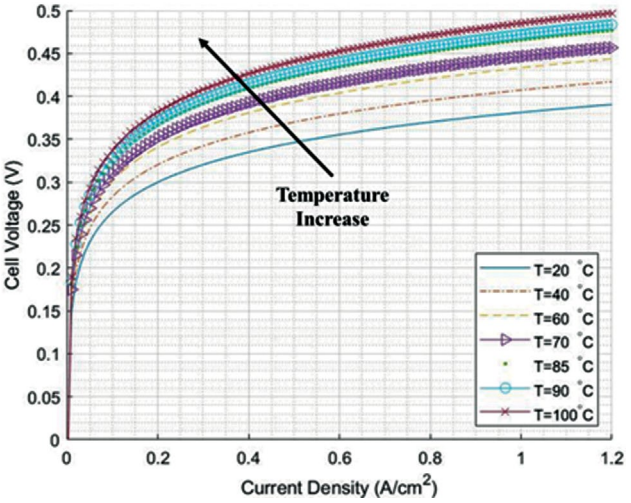


Figure 16. Plot of activation losses at different operating temperatures.

and thus decreasing the overall performance. To verify the behaviour of the power output, the same conclusions were obtained in [39].

Polarisation and Voltage Losses

Figure 15 shows the polarisation curve at different operating temperatures. From the plot, as the temperature increases the polarisation curve shifts downward to a lower voltage of a specific current density. This can be illustrated as the increase in temperature will result in an increase in the activation losses. Thus, decreasing the output voltage. Similar conclusion was obtained in literature but from an experimental work [40].

Studying the different voltage losses separately, to begin with, the activation losses. From Figure 16, it can be observed that raising the operating cell temperature will shift the activation losses plot upwards. Thus, the net voltage decreases due to the increase in the activation losses. This theoretical conclusion matches the work in [24].

Secondly, ohmic losses are related to the electrical resistance of the electrodes. There are four ways to reduce the internal resistance of the cell: the implementation of electrodes with the highest possible conductivity, good design, material selection of the bipolar plates or cell interconnects, and reducing the electrode's thickness [38]. Figure 17 shows the polarization curve with variation of electrolyte

thickness. The voltage output was higher at 100 μm than 700 μm of electrolyte thickness, which agrees with the point stated before. This conclusion matches [22]. This can be explained as electrolyte thickness directly affects the ohmic losses. Figure 18 shows the relation between ohmic losses and electrolyte thickness. It was obtained that as thickness increases, ohmic losses increase and thus the net voltage decreases, which results in lowering the power output of the system (as stated in the previous section). The same findings were obtained in [22].

Third, mass transfer losses (or mass concentration) occur when the rate of mass transport of a species to or from the electrode limits the available production. Mass transfer losses generally occur at high current densities due to limited mass transfer to the electrode by diffusion. There is no definitive analytical solution to the problem of modeling voltage changes that works satisfactorily in all cases [38]. It can be seen in Figure 19 that the mass transport losses remained zero until the current density reaches a value of 0.5 A/cm^2, then it started to increase exponentially. The same conclusion was obtained in [41].

After plotting all the losses curves separately, Figure 20 shows these losses combined. Activation losses have a major impact on the net voltage of the fuel cell with a logarithmic relationship with the current density. The ohmic losses have the least effect on the system voltage with a linear relation

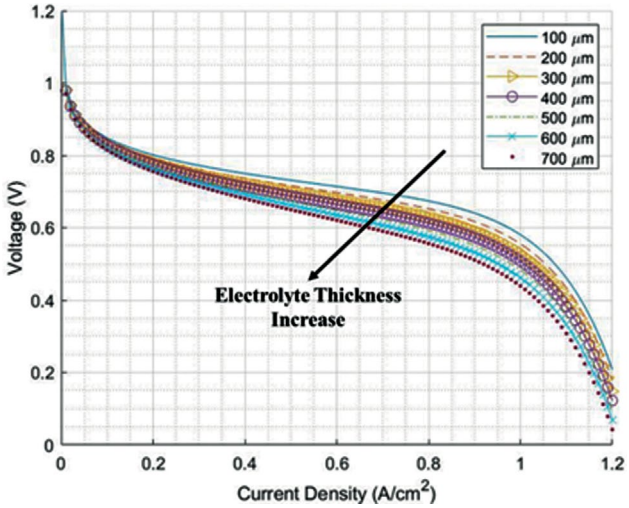


Figure 17. Plot of polarization curve with variation of electrolyte thickness.

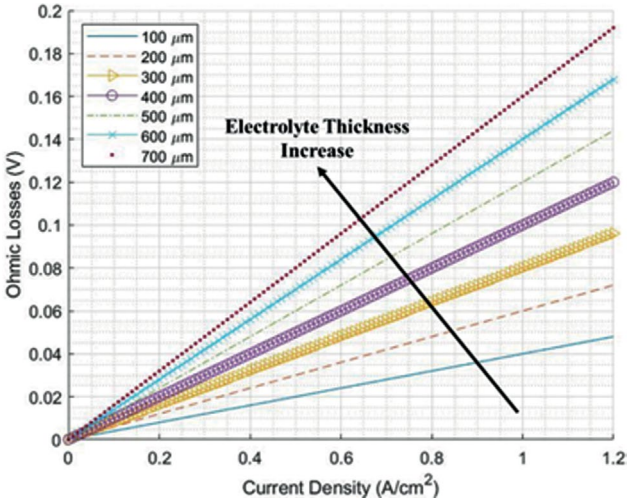


Figure 18. Plot of ohmic losses at different electrolyte thicknesses.

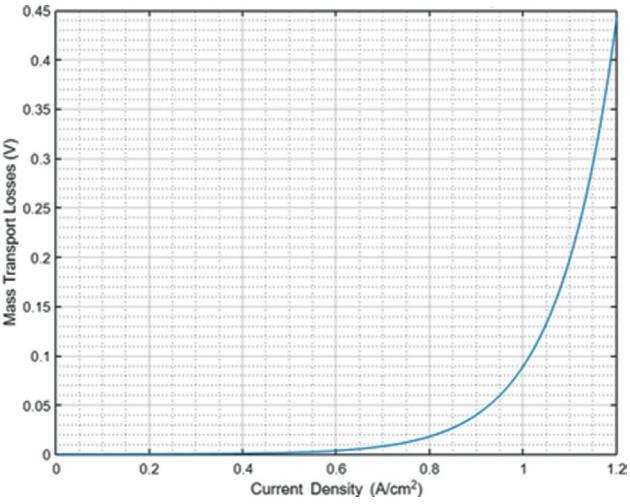


Figure 19. Plot of mass transport losses vs. current density.

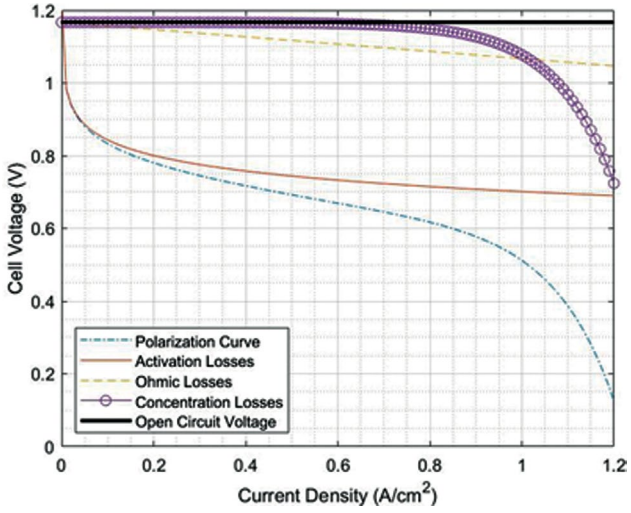


Figure 20. Plot of polarization curve.

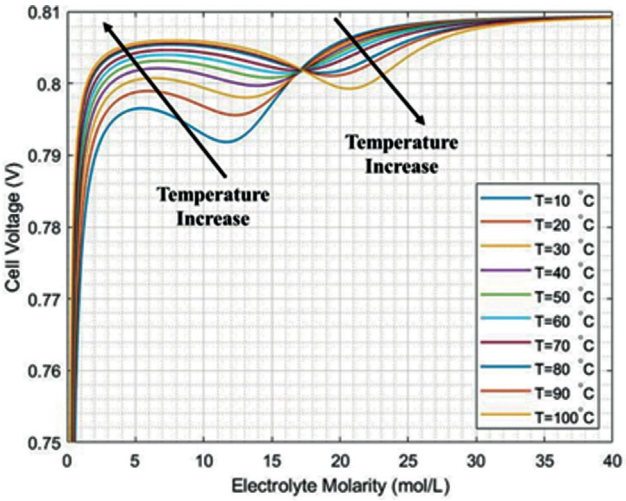


Figure 21. Plot of the voltage output vs. the KOH concentration.

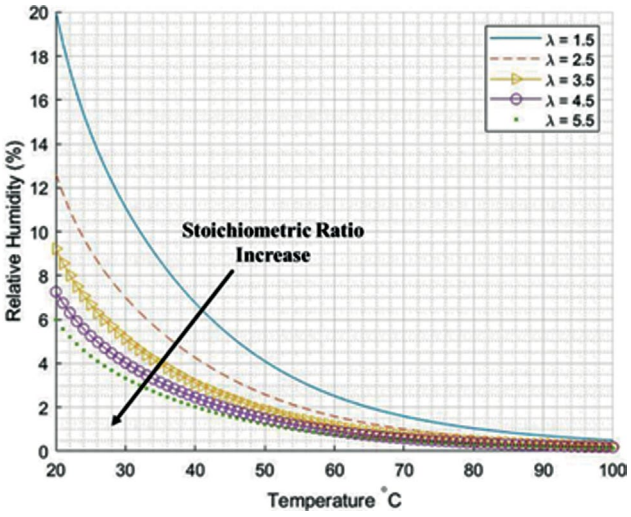


Figure 22. Plot of relative humidity vs. the temperature with variation of stoichiometry ratio of oxygen.

with the current density. Finally, the mass transportation losses are exponentially related to the current density.

Figure 21 shows the results of investigating the KOH concentration to assure the desired voltage at a certain operating temperature. It was found that as KOH concentration increases, the output voltage increases up to a turning point and then starts fluctuating onwards. At the same time, as temperature increases, the voltage increases up to a critical KOH concentration value, where the trend reverses after the critical value so that increasing temperature will result in dropping the output voltage. The original ΔV_{ohmic} considers the ohmic resistance due to several parameters such as the anode, cathode and contact area. However, the term "U_{ohm}" governs only the effect of the ohmic losses due to the KOH electrolyte concentration. The desired voltage is 0.8113 v. From the plot, the concentration to obtain this voltage was M_{plot} was found to be13.2 mol/L. A mathematical expression is used as verification to obtain the optimum concentration at a corresponding temperature of interest in equation (36). After plotting the temperature on the equation, M_{opt} was found to be 13.14 mol/L. The percentage difference obtained between M_{plot} and M_{opt} is equal to 0.394%, which shows accurate results and it matches the results obtained in [15].

Humidification and Pressure Drop

Maintaining the air humidity and the inlet and outlet water of the fuel cell enhances the fuel cell efficiency. According to [22], a well-humidified fuel cell improves the performance and increases the cell voltage because activation and ohmic losses decrease when humidity increases. Figure 22 shows the relative humidity and temperature with the variation in the stochiometric ratio of oxygen. It

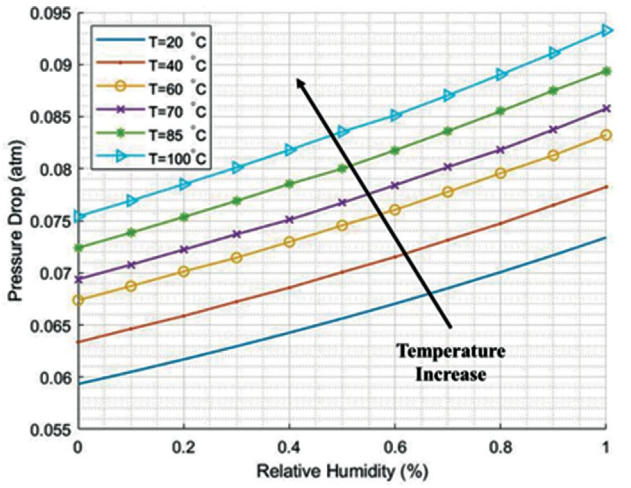


Figure 23. Plot of pressure drop vs. the relative humidity at different temperatures.

can be seen from the plot that humidity decreases with the increase in both the operating temperature and stochiometric ratio. The same trend is obtained from [42].

Figure 23 shows the relationship between pressure drop in the fuel cell and the relative humidity at different operating temperatures. It can be observed that relative humidity and pressure drop have a semi-linear increasing relationship. At the same time, when temperature increases, pressure drop also increases. Because uniformity of flow is a critical operational parameter, good pressure distribution ensures good reaction rates. Consequently, proper bipolar plate design is critical. The main parameters to focus on

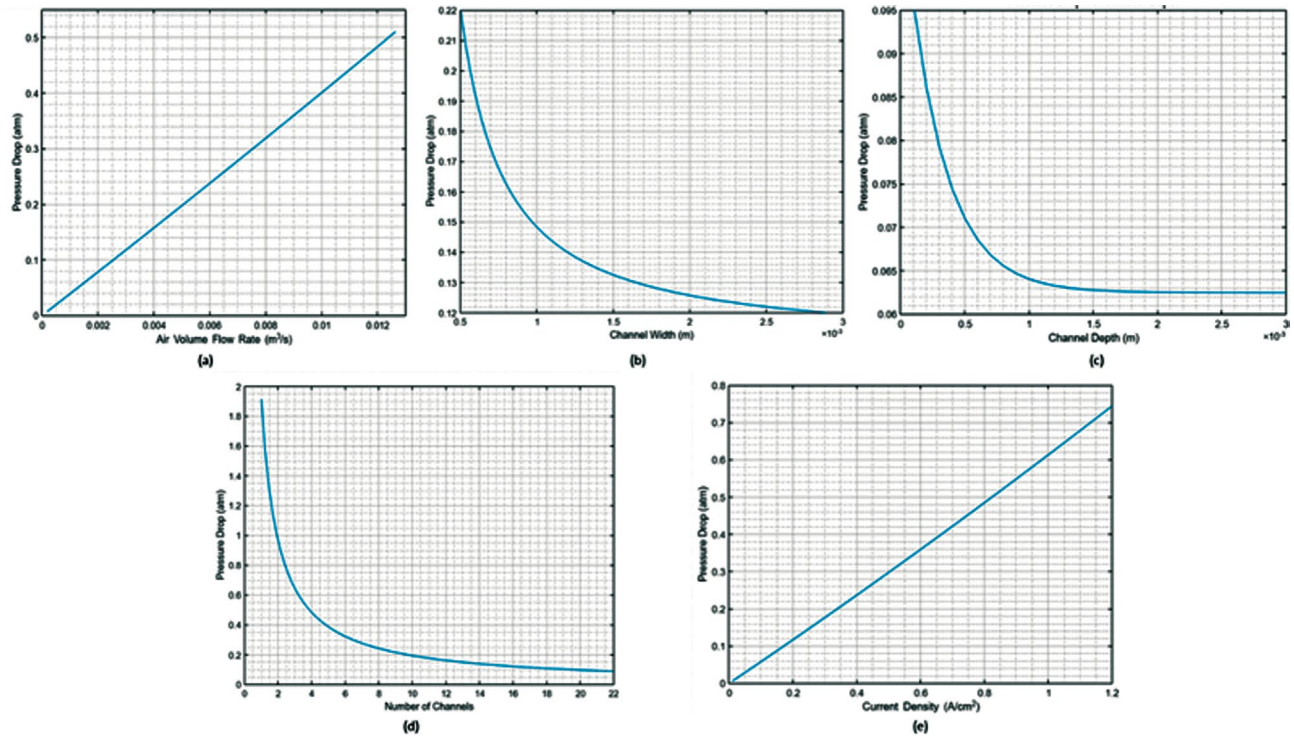


Figure 24. Pressure drop vs. (a) air volume flow Rate, (b) channel width, (c) channel depth, (d) number of channels, (e) current density.

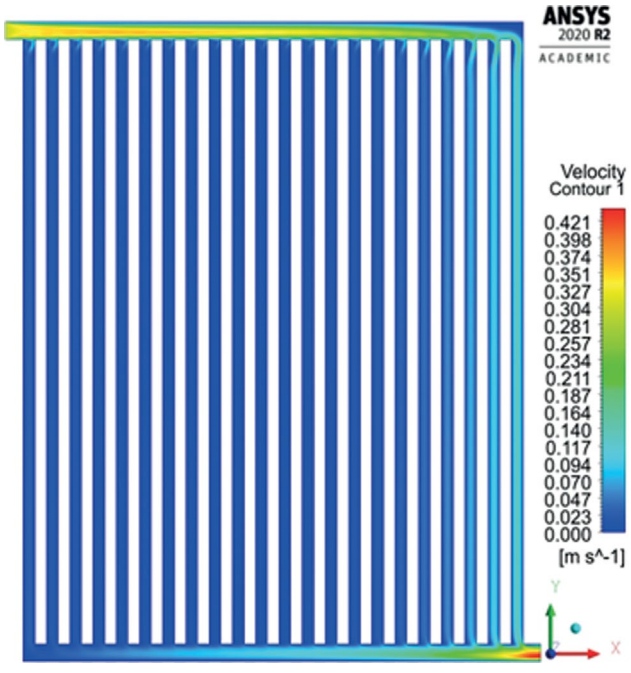


Figure 25. Velocity magnitude contour for air.

are relative humidity, volume flow rate, channel width and depth and the number of channels.

In Figure (24a), the plot shows the relationship between the pressure drop across the channels with the volumetric flow rate. The relationship between both is directly proportional following a semi-linear trend. As the flow rate increases, the pressure drop also increases; this is because, at higher velocities, more losses occur due to the nonuniform flow of the fluid. This drop is also due to the issue where the cathode struggles to completely absorb the water content that is present in vapour form. This leads to a fully humidified water droplet [4]. In Figures (24b), (24c) and (24d), the plots show the relationship between the pressure drop with the channel width, channel depth and the number of channels, respectively. The relationship is inversely proportional to a non-linear trend for the pressure with both the width and depth of the channel, because when increasing any of these two geometrical parameters, more cross-sectional area is available for the flow, which leads to a slower velocity of the fluid to maintain continuity. It was noticed that the change in the pressure drop was sharp for the number of channels starting from 2 channels till 12 channels. After 12 channels, pressure smoothly drops with almost negligible difference when increasing the number of channels. . Finally, Figure (24e) shows the relationship between the pressure drop and the current density. The relationship is directly proportional to a semi-linear trend. The same conclusions were obtained in [43].

Bipolar Plate CFD Simulations

Air was used as the working fluid in the CFD simulation. Figure 25 shows the mean velocity profile contours across the bipolar plate. At the channel inlet, the velocity is high as

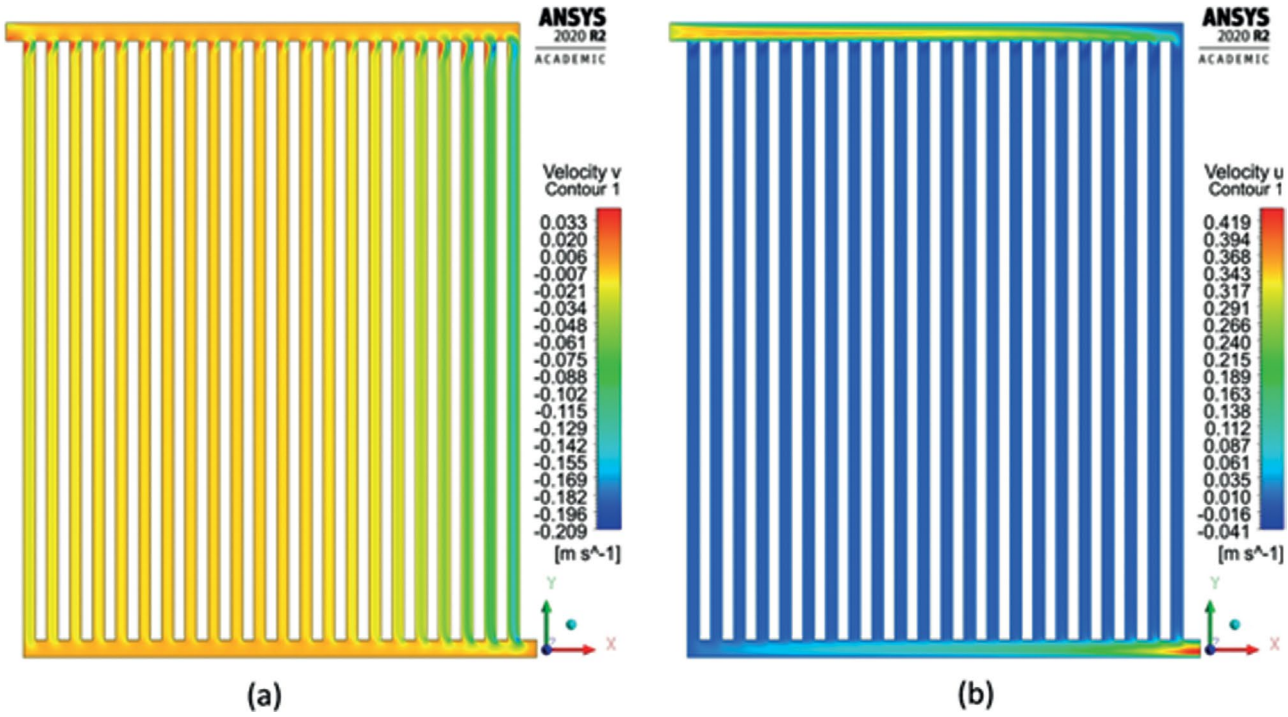


Figure 26. Contours of (a) y-velocity magnitude (b)x-velocity magnitude of air.

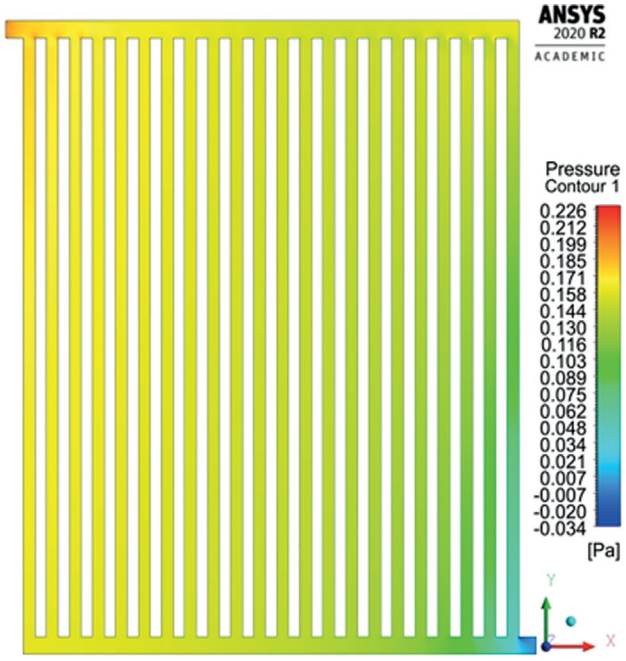


Figure 27. Contour of total pressure for air.

it is the injection point of the fluid, then, it tends to decrease at the horizontal wall due to the presence of shear stress which forces the fluid to develop boundary layers, In addition, gravity partially forces the fluid to start moving towards the vertical channels of the bipolar plates. It can be observed from the plot that the fluid tends to be a fully developed near the inlet. There are areas where the bipolar plate has relatively small velocities, due to the laminar flow behaviour. Then the fluid starts to accumulate again at the bottom section of the bipolar plate. Additionally, due to the presence of the stoichiometric ratio, there is a magnitude velocity at the output. The simulations performed in [35,44] had similar results and flow behaviour, higher velocities at the inlet and outlet faces and smaller velocity magnitudes in between. Similarly, Figures (26a) and (26b) show the contours of x-velocity and y-velocity, respectively. It was observed that the distribution is uniform from the inlet to the outlet through a constant trend to maintain mass conservation.

The total pressure is the pressure considering static and dynamic pressures. Static pressure is the pressure when the fluid is at rest, whereas dynamic pressure is when the fluid is in motion. Figure 27 shows the contours of the total pressure. It can be noticed that the pressure decreases as the fluid flows through the channels due to the losses between the fluid and the channels. This effect is also illustrated by the diffusion of the fluid towards the GDL. Channels and edges closer to the dead end of the inlet zone develop higher pressure drop than those farther away. The same conclusion can be related to the pressure drop obtained in [45].

CONCLUSION

In this paper, an alkaline fuel cell generates 10 kW of power to be deployed to supply electricity and water for a

one-day trip in a space mission application. The polarisation curve was plotted by considering the different types of voltage losses and the ways of reducing each loss' contribution on the overall performance.

Results showed that at 85 °C operating temperature, the maximum output voltage obtained theoretically was 0.8083 V at a corresponding current density of 150 mAcm^{-2}. The efficiency of the fuel cell system obtained was 74.8%.

CFD simulation was carried out to predict the velocity magnitude and total pressure contour distribution within the bipolar plate. Mesh independence validation was performed at different locations of the bipolar plate domain to ensure the accuracy of the data obtained. It was noticed that there were some zones where the velocity reaches almost zero, especially near the edges and corners. The total pressure was affected by the presence of the shear stress on the wall and the difference in pressure generated due to the physics of the bipolar plate's channel distribution.

Major conclusions obtained from the numerical analysis can be summarized as follows:

1. As operating temperature increases, voltage increases thus theoretical overall efficiency decreases.
2. Increasing the inlet fluid pressure will increase the output cell voltage which enhances the overall efficiency.
3. Activation losses can be reduced by changing the operating temperature.
4. Ohmic losses can be reduced by decreasing the thickness of internal components (electrolyte, anode, cathode or bipolar plate)
5. The power output has a critical value at a certain current density (in our work, it was 1 Acm^{-2})
6. Optimum KOH concentration was found to be M_{plot}=13.2 mol/L. As KOH concentration increases, the output voltage increases up to a turning point and then starts fluctuating.
7. Pressure drop across the bipolar plate is proportional with air volume flow rate and current density. In contrast, pressure drop is inversely proportional with channel width, channel depth and number of channels.
8. End zones in bipolar plates are more likely accumulating higher pressure and lower velocity magnitude.

In future works, GDL effect will be taken in consideration to understand the effect of the diffusion equations on the performance of AFC. To perform the work, GDL with porous layers must be installed in the design to achieve the futuristic objectives. Secondly, life cycle assessment of AFC must be performed in every stage of operating AFC. For example, material selection, manufacturing and end of life applications.

NOMENCLATURE

A_{cell}	Active Surface Area (cm^2)
C	Mesh Quality Constant
c_p	Specific Heat (kJ kg^{-1}K^{-1})
D_H	Hydraulic Diameter (m)
E	Pressure and Concentration Voltage (V)
$Edge\ legth$	Calculated Mesh Edge Length
G	Pressure and Concentration Gibbs (J kg^{-1})
g_x, g_y, g_z	Gravitational vector component in x,y,z -directions (m s^{-2})
ΔG	Total Gibbs free energy (J kg^{-1})
ΔH	Total Enthalpy of Formation (J kg^{-1})
h	Enthalpy (J mol^{-1})
$H_{2,usage}$	Minimum Hydrogen needed (kg s^{-1})
h	Height of The Fuel Cell (cm)
i	Current Density (A cm^{-2})
$i_{o_}a$	Anode Exchange Current Density (A cm^{-1})
$i_{o_}c$	Cathode Exchange Current Density (Acm^{-1})
i_x	Internal Current Density (A cm^{-2})
I	Current (A)
K_L	Minor Losses Factor
k	Specific Conductivity of KOH Electrolyte
k_m	Material Conductivity (W m^{-1} k^{-1})
l_a	Length of Anode (m)
l_e	Length of Electrolyte (m)
l_c	Length of Cathode (m)
m	Transportation Losses Constant (V)
m_{O_2}	Oxygen Mass (kg)
M_{plot}	Molarity Obtained from Plot (mol L^{-1})
M_{opt}	Molarity Obtained from Equation (mol L^{-1})
n	Transportation Losses Constant (cm^2 A^{-1})
N_{cells}	Number of Cells in Stack
$\dot{n}$	Molar Rate (mol s^{-1})
$O_{2,usage}$	Minimum Oxygen Needed
P	Partial Pressure (atm)
$P_{sat@T_{in}}$	Saturation Pressure (atm)
ΔP	Pressure Drop (atm)
P	Power Output (W)
$Q_{st,in}$	Volumetric Flow (m^3 s^{-1})
$Quality$	Calculated Mesh Quality
r	Volume Fraction
R	Anode, Cathode Resistance (Ω cm^2)
ΔS	Total Entropy Change (J kg^{-1} K^{-1})
s	Entropy (J kg^{-1} K^{-1})
T	Operating Temperature (K)
U_{ohm}	Ohmic Losses Due to Concentration (V)
V	True Voltage Value (V)
V_C	Cell Voltage (V)
ΔV_{act}	Activation Losses Voltage (V)
ΔV_{ohm}	Ohmic Losses Voltage (V)
ΔV_{trans}	Transportation Losses Voltage (V)
v_{avg}	Average Velocity of Fluid (m s^{-1})
$volume$	Calculated Mesh Element Volume
w	Width of The Fuel Cell (cm)

z	Number of Electrons
$\frac{\partial(u)}{\partial x}, \frac{\partial(v)}{\partial x}, \frac{\partial(w)}{\partial x}$	Differential Variation of u,v,w Velocity Components in X-Direction
$\frac{\partial(u)}{\partial y}, \frac{\partial(v)}{\partial y}, \frac{\partial(w)}{\partial y}$	Differential Variation of u,v,w Velocity Components in Y-Direction
$\frac{\partial(u)}{\partial z}, \frac{\partial(v)}{\partial z}, \frac{\partial(w)}{\partial z}$	Differential Variation of u,v,w Velocity Components in Z-Direction
$\frac{\partial^2 T}{\partial x^2}, \frac{\partial^2 T}{\partial y^2}, \frac{\partial^2 T}{\partial z^2}$	Second Differential of Temperature in x,y,z-Directions
$\frac{\partial P}{\partial x}, \frac{\partial P}{\partial y}, \frac{\partial P}{\partial z}$	Differential Variation of Pressure in x,y,z - Direction

Greeks

μ_f	Fuel Utilization Factor
ρ	Density of Fluid (kg m^{-3})
f	Darcy Friction Loss Factor
λ	Stoichiometry Ratio
α	Charge Transfer Coefficient
$\sigma_a, \sigma_e, \sigma_c$	Conductivity of Anode, Electrolyte, Cathode (S m^{-1})
φ	Humidity of Fluid (%)

Abbreviations

AFC	Alkaline Fuel Cell
BoP	Balance of Plant
BP	Bipolar Plates
CFD	Computational Fluid Dynamics
EMF	Electromotive Force (V)
GDL	Gas Diffusion Layer
HHV	Higher Heating Value (kJ/kmol)
KOH	Potassium Hydroxide
LW	Land to Channel Ratio
MEA	Membrane Electrode Assembly
MW	Molar Weight (g mol^{-1})
Re	Reynolds Number
RH	Relative Humidity

Constants

F	Faraday Constant = 96,500 (C mol^{-1})
R	Universal Gas Constant = 8.3144 (J mol^{-1} K^{-1})
g	Gravimetric Acceleration = 9.81 (m s^{-2})

AUTHORSHIP CONTRIBUTIONS

Authors equally contributed to this work.

DATA AVAILABILITY STATEMENT

The authors confirm that the data that supports the findings of this study are available within the article. Raw data that support the finding of this study are available from the corresponding author, upon reasonable request.

CONFLICT OF INTEREST

The author declared no potential conflicts of interest with respect to the research, authorship, and/or publication of this article.

ETHICS

There are no ethical issues with the publication of this manuscript.

REFERENCES

[1] Ministry of Climate Change and Environment. UAE National air emissions inventory project - Final results. Available at: https://www.moccae.gov.ae/assets/download/fa2f8dd4/Air Emissions Inventory Report.pdf.aspx?view=true Accessed on February 16, 2020.

[2] The United Arab Emirates' Government Portal. The UAE's response to climate change. Available at: https://u.ae/en/information-and-services/environment-and-energy/climate-change/theuaesresponse-toclimatechange Accessed on March 26, 2021.

[3] Twinkle Toes Engineering. Hydrogen fuel cell car. Available at: http://www.twinkletoesengineering.info/hydrogen_car.htm Accessed on 26, March, 2021.

[4] Sharaf OZ, Orhan MF. An overview of fuel cell technology: Fundamentals and applications. Renew Sustain Energy Rev 2014;32:810–853. [CrossRef]

[5] Brandon N, Hart D. An introduction to fuel cell technology and economics Centre for Energy Policy and Technology 1999.

[6] Merle G, Wessling M, Nijmeijer K. Anion exchange membranes for alkaline fuel cells: A review. J Memb Sci 2011;377:1–35. [CrossRef]

[7] Shah RK, Desideri U, Hsueh KL, Vikar A V, Sunden B, Vilemas J. Research opportunities and challenges in fuel cell science and engineering. Adv Heat Transf Eng Proc 2003.

[8] Brandon NP. Fuel cells: Materials. In: Buschow KHJ, Flemings MC, Kramer EJ, Cahn RW, Mahajan S, et al, editors. Encyclopedia of materials: Science and technology. 2nd ed. Oxford:Pergamon Press; 2004. p. 1–5.

[9] Djilali N, Mclean GF, Niet T, Prince-Richard S, Djilali N. An assessment of alkaline fuel cell technology. Int J Hydrog Energy 2002;27:507–526. [CrossRef]

[10] Baroutaji A, Carton JG, Sajjia M, Olabi AG. Materials in PEM fuel cells. Elsevier Ltd.; 2016. https://doi.org/10.1016/b978-0-12-803581-8.04006-6. [CrossRef]

[11] Lee HS, Yu JK, Kim JY, Kim KH, Rhee YW. Effects of catalyst loading and oxidant on the performance of direct formic acid fuel cells. Stud Surf Sci Catal 2006;159:589–592. [CrossRef]

[12] Abderezzak B. Introduction to hydrogen technology. In: editor. Introduction to transfer Phenomena in PEM fuel cell. 1st ed. London: ISTE Press-Elsevier; 2018. p. 1–51. [CrossRef]
[13] Li YS, Zhao TS, Chen R. Cathode flooding behaviour in alkaline direct ethanol fuel cells. J Power Sources 2011;196:133–139. [CrossRef]
[14] Dincer I, Acar C. Review and evaluation of hydrogen production methods for better sustainability. Int J Hydrog Energy 2014;40:11094–11111. [CrossRef]
[15] Verhaert I, De Paepe M, Mulder G. Thermodynamic model for an alkaline fuel cell. J Power Sources 2009;193:233–240. [CrossRef]
[16] Zhang H, Lin G, Chen J. The performance analysis and multi-objective optimization of a typical alkaline fuel cell. Energy 2011;36:4327–4332. [CrossRef]
[17] Sommer EM, Martins LS, Vargas JVC, Gardolinski JEFC, Ordonez JC, Marino CEB. Alkaline membrane fuel cell (AMFC) modeling and experimental validation. J Power Sources 2012;213:16–30. [CrossRef]
[18] Mulder G, Coenen P, Martens A, Spaepen J. The development of a 6 kW fuel cell generator based on alkaline fuel cell technology. Int J Hydrog Energy 2008;33:3220–3224. [CrossRef]
[19] Ziems C, Tannert D, Krautz HJ. Project presentation: Design and installation of advanced high pressure alkaline electrolyzer-prototypes. Energy Procedia 2012;29:744–753. [CrossRef]
[20] Verhaert I, Verhelst S, Huisseune H, Poels I, Janssen G, Mulder G, et al. Thermal and electrical performance of an alkaline fuel cell. Appl Therm Eng 2012;40:227–235. [CrossRef]
[21] Verhaert I, Verhelst S, Janssen G, Mulder G, De Paepe M. Water management in an alkaline fuel cell. Int J Hydrog Energy 2011;36:11011–11024. [CrossRef]
[22] Jiao K, Huo S, Zu M, Jiao D, Chen J, Du Q. An analytical model for hydrogen alkaline anion exchange membrane fuel cell. Int J Hydrog Energy 2015;40:3300–3312. [CrossRef]
[23] Ariyanfar L, Ghadamian H, Roshandel R. Alkaline fuel cell (AFC) engineering design, modeling and simulation for UPS provide in laboratory application. In: Moshfegh B, editor. World Renewable Energy Congress; 2011 May 8-13; Linköping, Sweden: 2011. pp. 1227–1234. [CrossRef]
[24] Lin BYS, Kirk DW, Thorpe SJ. Performance of alkaline fuel cells: A possible future energy system? J Power Sources 2006;161:474–483. [CrossRef]
[25] Wang YJ, Qiao J, Baker R, Zhang J. Alkaline polymer electrolyte membranes for fuel cell applications. Chem Soc Rev 2013;42:5768–5787. [CrossRef]
[26] Liu L, Yao L, Feng K, Luo Z, Liu K, Zhu H, et al. In silico screening and design of coating materials for PEMFC bipolar plates. Coatings 2018;8:1–10.
[27] Britannica. Fuel cell - Types of fuel cells. Available at: https://www.britannica.com/technology/fuel-cell/Types-of-fuel-cells Accessed on March 26, 2021.
[28] Hermann A, Chaudhuri T, Spagnol P. Bipolar plates for PEM fuel cells: A review. Int J Hydrog Energy 2005;30:1297–1302. [CrossRef]
[29] Global Alkaline Fuel Cell (AFC) Market 2020 by Manufacturers, Regions, Type and Application, Forecast to 2025 | Market Research Reports® Inc. n.d. https://www.marketresearchreports.com/gir/global-alkaline-fuel-cell-afc-market-2020-manufacturers-regions-type-and-application-forecast (accessed March 26, 2021).
[30] Larminie J, Dicks A. Fuel Cell Systems Explained. 2nd edition. Oxford, Brisbane: John Wiley & Sons Ltd; 2003. [CrossRef]
[31] Low contact resistance | Plating technologies n.d. https://www.oms.co.jp/en/service/plating-tec/plating2/cat8/ (accessed March 26, 2021).
[32] Meltric. Decontactor™ Technology. Available at: https://meltric.com/products/decontactor-technology Accessed on March 26, 2021.
[33] Peng L, Lai X, Liu D, Hu P, Ni J. Flow channel shape optimum design for hydroformed metal bipolar plate in PEM fuel cell. J Power Sources 2008;178:223–230. [CrossRef]
[34] Mohammadi M, Jovanovic GN, Sharp KV. Numerical study of flow uniformity and pressure characteristics within a microchannel array with triangular manifolds. Comput Chem Eng 2013;52:134–144. [CrossRef]
[35] Imbrioscia GM, Fasoli HJ. Simulation and study of proposed modifications over straight-parallel flow field design. Int J Hydrog Energy 2014;39:8861–8867. [CrossRef]
[36] Cerón-Bretón JG, Cerón-Bretón RM, Rangel-Marrón M, Muriel-García M, Cordova-QuirozA.V., Estrella-Cahuich A. Prediction and optimization of fuel cell performance using a multi-objective genetic algorithm. Int J Hydrogen Energy 2011;5:328–36.
[37] EG&G Technical Services Inc. Fuel Cell Handbook. 7th ed. Morgantown, West Virginia: U.S. Department of Energy; 2004. https://doi.org/10.1016/s0031-9422(00)82398-5. [CrossRef]
[38] Mench MM. Fuel Cell Engines. 1st ed. New York: John Wiley & Sons; 2008. [CrossRef]
[39] Sarapuu A, Kibena-Põldsepp E, Borghei M, Tammeveski K. Electrocatalysis of oxygen reduction on heteroatom-doped nanocarbons and transition metal-nitrogen-carbon catalysts for alkaline membrane fuel cells. J Mater Chem A 2018;6:776–804. [CrossRef]
[40] Amores E, Rodríguez J, Oviedo J, De Lucas-Consuegra A. Development of an operation strategy for hydrogen production using solar PV

energy based on fluid dynamic aspects. Open Eng 2017;7:141–152. [CrossRef]

[41] Winterbone DE, Turan A. Fuel Cells. In: editor. Advanced thermodynamics for engineers. 2nd ed. Oxford: Butterworth-Heinemann; 2015. p. 497–526. [CrossRef]

[42] Engineering ToolBox. Moist air - Weight of water vapor. Available at: https://www.engineeringtoolbox.com/water-vapor-air-d_854.html. Accessed on March 27, 2021.

[43] Kahraman H, Orhan MF. Flow field bipolar plates in a proton exchange membrane fuel cell: Analysis & modeling. Energy Convers Manag 2017;133:363–384. [CrossRef]

[44] Arbabi F, Roshandel R, Moghaddam GK. Numerical modeling of an innovative bipolar plate design based on the leaf venation patterns for PEM fuel cells. Int J Eng 2012;25:177–186. [CrossRef]

[45] Edupuganti V. An Investigation of the Impact of the Proton Exchange Membrane Fuel Cell Flow Field Plate Geometry and Design Using Computational Fluid Dynamic Modeling and Simulation 2012.